NASA/CR–2001–211266

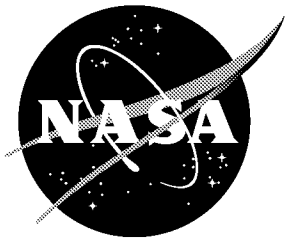

An Inviscid Computational Study of Three '07 Mars Lander Aeroshell Configurations Over a Mach Number Range of 2.3 to 4.5

Ramadas K. Prabhu
Lockheed Martin Engineering & Sciences Company, Hampton, Virginia

December 2001

The NASA STI Program Office ... in Profile

Since its founding, NASA has been dedicated to the advancement of aeronautics and space science. The NASA Scientific and Technical Information (STI) Program Office plays a key part in helping NASA maintain this important role.

The NASA STI Program Office is operated by Langley Research Center, the lead center for NASA's scientific and technical information. The NASA STI Program Office provides access to the NASA STI Database, the largest collection of aeronautical and space science STI in the world. The Program Office is also NASA's institutional mechanism for disseminating the results of its research and development activities. These results are published by NASA in the NASA STI Report Series, which includes the following report types:

- TECHNICAL PUBLICATION. Reports of completed research or a major significant phase of research that present the results of NASA programs and include extensive data or theoretical analysis. Includes compilations of significant scientific and technical data and information deemed to be of continuing reference value. NASA counter-part of peer-reviewed formal professional papers, but having less stringent limitations on manuscript length and extent of graphic presentations.

- TECHNICAL MEMORANDUM. Scientific and technical findings that are preliminary or of specialized interest, e.g., quick release reports, working papers, and bibliographies that contain minimal annotation. Does not contain extensive analysis.

- CONTRACTOR REPORT. Scientific and technical findings by NASA-sponsored contractors and grantees.

- CONFERENCE PUBLICATION. Collected papers from scientific and technical conferences, symposia, seminars, or other meetings sponsored or co-sponsored by NASA.

- SPECIAL PUBLICATION. Scientific, technical, or historical information from NASA programs, projects, and missions, often concerned with subjects having substantial public interest.

- TECHNICAL TRANSLATION. English-language translations of foreign scientific and technical material pertinent to NASA's mission.

Specialized services that help round out the STI Program Office's diverse offerings include creating custom thesauri, building customized databases, organizing and publishing research results... even providing videos.

For more information about the NASA STI Program Office, see the following:

- Access the NASA STI Program Home Page at ***http://www.sti.nasa.gov***

- E-mail your question via the Internet to help@sti.nasa.gov

- Fax your question to the NASA Access Help Desk at (301) 621–0134

- Phone the NASA Access Help Desk at (301) 621–0390

- Write to:
  NASA Access Help Desk
  NASA Center for AeroSpace Information
  7121 Standard Drive
  Hanover, MD 21076–1320

NASA/CR–2001–211266

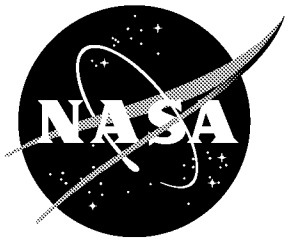

An Inviscid Computational Study of Three '07 Mars Lander Aeroshell Configurations Over a Mach Number Range of 2.3 to 4.5

Ramadas K. Prabhu
Lockheed Martin Engineering & Sciences Company, Hampton, Virginia

National Aeronautics and
Space Administration

Langley Research Center
Hampton, Virginia 23681–2199

Prepared for Langley Reseach Center
under contract NAS1-00135

December 2001

Available from the following:

NASA Center for AeroSpace Information (CASI)
7121 Standard Drive
Hanover, MD 21076–1320
(301) 621–0390

National Technical Information Service (NTIS)
5285 Port Royal Road
Springfield, VA 22161–2171
(703) 487–4650

Summary

This report documents the results of a study conducted to compute the inviscid longitudinal aerodynamic characteristics of three aeroshell configurations with trim tabs of the proposed '07 Mars lander. This was done in support of the activity to design a smart lander for the proposed '07 Mars mission. In addition to the three configurations designated as the 'shelf', the 'canted', and the 'Ames', the baseline configuration (without tab) was also studied. The unstructured grid inviscid CFD software FELISA was used, and the longitudinal aerodynamic characteristics of the four configurations were computed for Mach number of 2.3, 2.7, 3.5, and 4.5, and for an angle of attack range of -4 to 20 degrees. Wind tunnel tests had been conducted on scale models of these four configurations in the Unitary Plan Wind Tunnel, NASA Langley Research Center. Present computational results are compared with the data from these tests. Some differences are noticed between the two results, particularly at the lower Mach numbers. These differences are attributed to the pressures acting on the aft body. Most of the present computations were done on the forebody only. Additional computations were done on the full body (forbody and aftbody) for the baseline and the 'Shelf' configurations. Results of some computations done (to simulate flight conditions) with the Mars gas option and with an "effective" γ are also included.

Nomenclature

C_A	$\mathbf{F_A}/(q_\infty\ S_{ref})$, Axial force coefficient
C_D	$C_A\ cos(\alpha)\ +\ C_N\ sin(\alpha)$, Drag coefficient
C_N	$\mathbf{F_N}/(q_\infty\ S_{ref})$, Normal force coefficient
C_L	$C_N\ cos(\alpha)$ - $C_A\ sin(\alpha)$, Lift coefficient
C_m	$\mathbf{M_y}/(q_\infty\ S_{ref}\ l_{ref})$, Pitching moment coefficient
C_p	$(p$ - $p_\infty)/q_\infty$, Pressure coefficient
$\mathbf{F_A}$	Axial force
$\mathbf{F_N}$	Normal force
l_{ref}	Reference length
L/D	C_L/C_D
$\mathbf{M_y}$	Pitching moment
M_∞	Freestream Mach number
p	Static pressure
p_∞	Freestream static pressure
q_∞	Freestream dynamic pressure
S_{ref}	Reference area
x, y, z	Cartesian co-ordinates of a given point
α	Angle of attack, deg.
γ	Isentropic index

Introduction

The second generation or "smart" landers planned for '07 Mars mission are capable of performing precision landing, hazard avoidance, and hazard tolerance. (see Ref. [1]) The primary aerodynamic requirement for such a smart lander is that it should produce an L/D of -0.22 to 0.25 at the trim angle of attack. In an extensive study aimed at arriving a suitable shape for the aeroshell several shapes had been screened [2]. As a result of this study, two configurations were down-selected, and detailed study was done to compute their aerodynamics characteristics over a Mach number range. (see Ref. [3]) Ballistic tests had been done on a related configurations considered to be a possible candidate. Low supersonic wind tunnel test were done in the NASA Unitary Plan Wind Tunnel on the three candidate aeroshell configuration and also on the baseline configuration. Longitudinal aerodynamic characteristics were measured for Mach 2.3, 2.7, 3.5, and 4.5 over an angle of attack of -5 to +20 degrees. A limited number of asymmetric tests were also done to measure the lateral and directional aerodynamic characteristics. In order to supplement this data, a detailed set of inviscid flow computations were done using the software FELISA [4], and longitudinal aerodynamic characteristics of the four shapes were computed for 2.3, 2.7, 3.5, and 4.5 over an angle of attack of -5–+20 degrees. The present report presents these results and also shows a comparison with the wind tunnel data. Flow conditions in the Unitary Plan Wind Tunnel are quite different from the flight conditions in the Mars atmosphere for the same Mach number. Therefore, a few additional computations were done with flow conditions simulating flight in Mars atmospheric gas.

Geometry

The present computational study was done for three aeroshell configurations for the proposed '07 Mars Lander. These are designated as the 'shelf', the 'canted', and the 'Ames' configurations. Each of these three configurations has a tab that makes them trim at non-zero angle of attack. In addition, the baseline configuration (no tab) was also studied. A sketch of the the four configurations is shown in Fig. 1. Axis system used for this study is also shown in the figure. The origin is at the nose of the body with the z-axis along the body axis pointing upstream, the x-axis in the symmetry plane perpendicular to the z-axis, and the y-axis perpendicular to the symmetry plane. The baseline geometry is a 4.05 m. diameter blunt conical forebody with a 70-deg. half-cone angle. The nose radius is 0.985 m. and the shoulder radius is 0.0987 m. In the 'shelf' and the 'Ames' configurations, the tab is an extension of the conical surface, whereas in the 'canted' configuration the tab is canted forward so that the tab make a 10 deg. angle with the conical surface. Since all these shapes are symmetric about the x-z plane, only one half of these bodies were simulated in the computational model. The reference quantities used for reducing the aerodynamic loads to the non-dimensional form are as follows:

Reference area	12.8825 sq.m.
Reference length	4.05 m.
Pitching moment reference point	(0.0, 0.0, -0.8659) m.

The Felisa Software

Computations of the present study were done using the FELISA unstructured grid software. This software package consists of a set of computer codes for unstructured grid generation, and the simulation of

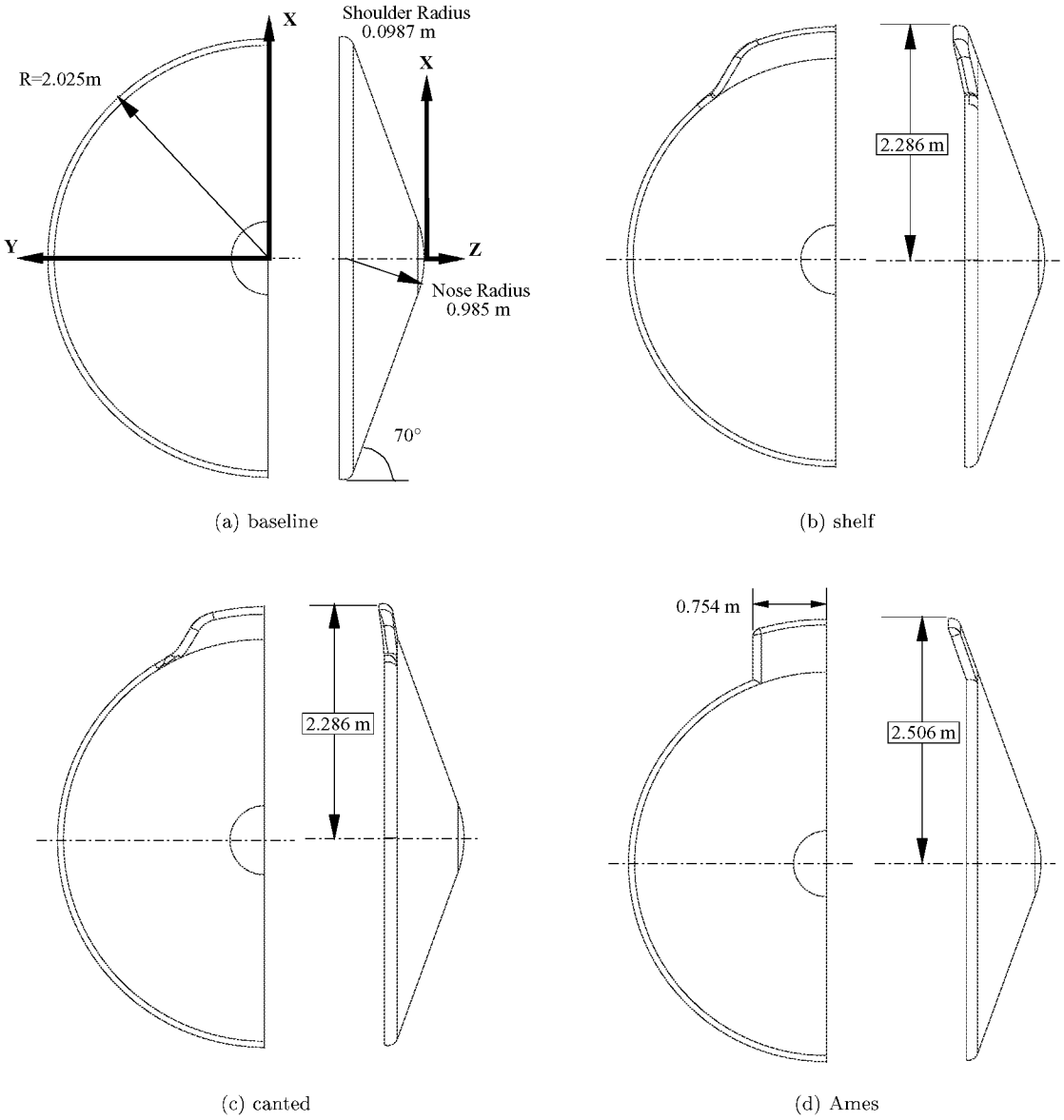

(a) baseline

(b) shelf

(c) canted

(d) Ames

Figure 1: Geometrical details of the four shapes

three-dimensional steady inviscid flows using unstructured tetrahedral grids. Surface triangulation and discretization of the computational domain using tetrahedral elements is done by using two separate codes. Two flow solvers are available—one applicable for transonic flows, and the other for hypersonic flows. The hypersonic flow solver has options for perfect gas, equilibrium air, CF_4, CO_2, and equilibrium Mars gases. This solver also has the capability of solving chemical non-equilibrium flow, and real gas (chemical and thermal non-equilibrium) flow. The hypersonic flow solver with the perfect gas (constant γ) and with the equilibrium Mars gas options was used for the present computations. Post-processors like the aerodynamic analysis routine are part of the software package. More information on FELISA software may be found in [4]. A description of the hypersonic flow solver may be found in [5].

Grids Used in the Present Study

Starting with the geometry files for the bodies in the iges format, and using the software GridTool [6], a set of FELISA data files was generated. These files include (1) the FELISA data file that contains all the information on the body surface definition and the computational domain in a format suitable for the FELISA grid generator, (2) the FELISA background file that specifies the grid spacing, and (3) the FELISA boundary conditions files. The minimum spacing for all the grids was 0.03 m. The computational domain was chosen to be sufficiently large so that the inflow boundaries would not affect the flow on the body. The computational domain used for the baseline configuration is shown in Figures 2. Similar computational domains were used for the other three configurations. The computational domain used for the full body configuration with a sting (as tested in the wind tunnel) is shown in Figures 3. Note, the size shown is the full scale vehicle size and not the model size actually tested in the wind tunnel. Also, the computational domian used for the full body and no sting is shown in Figures 4. Only a few computations were done with these configurations.

Using the FELISA data files, unstructured surface triangulation and tetrahedral grids were generated using the surface and volume grid generators, respectively. A single grid was built for each configuration. The properties of these grids are shown in Table 1. All these grids were generated on an SGI ONYX located in the Aerothermodynamics Branch (AB), NASA Langley Research Center.

Configuration	**No. of Tets**	**No. of Points**	**No. of Triangles**	**No. of Surface Points**
caseline	9,625,582	1,613,402	9,661	18,477
shelf	9,752,333	1,63,4514	10,124	19,119
canted	9,168,056	1,536,015	11,754	22,131
Ames	9,775,839	1,638,302	10,046	19,092

Table 1: Properties of grids used in the present computations.

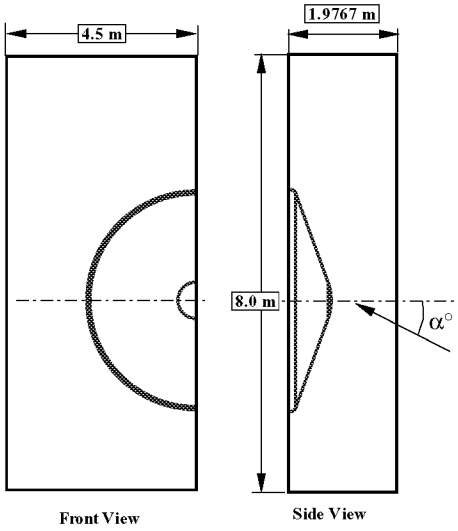

Figure 2: Computational domain for the forebody.

Flow Conditions

The four configurations analyzed here had been tested in the NASA Langley Unitary Plan Wind Tunnel. The total temperature in the tunnel test section during these tests was about 350 K. At this low temperature, air can be treated as perfect gas with $\gamma = 1.4$. Therefore, in order to compare the computational results with the wind tunnel data, a set of the computations were done with the assumption of perfect gas with $\gamma = 1.4$. Subsequent to this, a few more computations were done for Mach 4.5 freestream with equilibrium Mars gas and also with an effective γ. This was done to simulate the flight conditions in Mars atmosphere. The effective γ is defined as the value of the isentropic index that produces a normal-shock-density-ratio the same as that in equilibrium Mars gas. This values depends on the freestream Mach number; for Mach 4.5 the value of effective γ is 1.24.

Flow Solution

The flow solutions were computed on an SGI Origin 2000 class parallel computer. The grids were partitioned so that the problem would run on 64 processors. The FELISA hypersonic flow solver with the perfect gas option with $\gamma = 1.4$, was used for the initial computations. As noted earlier, some cases with the equilibrium Mars gas, and an effective $\gamma = 1.24$ were also done. Each solution was started with the low-order option, and after a few hundred iterations, the higher-order option was turned on, and the solution was run to convergence. After every 100 iteration, the surface pressures were integrated, and the aerodynamic loads, namely the normal and the axial forces, and the pitching moment acting on the body were computed. The

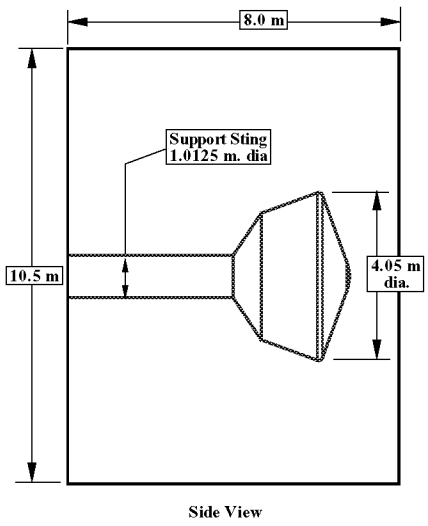

Figure 3: Computational domain for the wind tunnel model.

flow solution was assumed to be converged when these integrated loads reached steady values. The grids for the forebody required about 45 CPU-hours, whereas the grids for the wind tunnel model configuration required about 80 CPU-hours. It may be recalled that the wind tunnel model configuration has the aftbody and the support sting, and a much larger computational domain. The flow over the aftbody tends to be oscillatory, with more iterations required to reach convergence. The computed flow solutions were post-processed to obtain the aerodynamic loads. These loads were non-dimensionalized in the conventional manner, and the aerodynamic coefficients (C_N, C_A, C_L, C_D, L/D, and C_m) were obtained.

It should be recalled at this point that the present computations are inviscid; hence the viscous effects - skin friction and boundary layer separation are absent. For blunt bodies like the ones studied in this report, skin friction is a negligible part of the total force on the forebody. Therefore, the present results should predict the forebody aerodynamic loads well. Flow over the aftbody is viscous dominated, and because of abrupt changes in the surface slopes and the rearward facing surfaces, there would be separation on the the aftbody. This precludes simulation of such flows using inviscid flow solvers. However, the 'numerical viscosity' inherent in inviscid computations sometimes allow such flows to be computed. The resulting flow field shows features of a 'separated' flow. However, results of such computations should be treated with caution.

Results and Discussion

Aerodynamic coefficients from the present computations on the baseline, the 'shelf', the 'canted', and the 'Ames' configurations are summarized in Tables 2–7. Wind tunnel test data in tabular form for C_A, C_N,

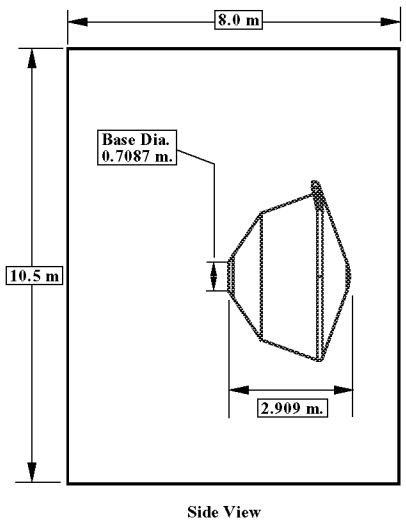

Figure 4: Computational domain for the full model with no sting.

C_m, C_L, C_D, and L/D are available for Mach 2.3, 2.7, 3.5, and 4.5 and α from -5 to +20 degrees for the four configurations, with the exception of the 'Ames' configuration for which test results are not available for Mach 4.5. In the following sections present computational results are compared with the wind tunnel data. Wherever differences are noticed, possible causes are identified. Results of additional computations in the wind tunnel model configuration (full model with a support sting) and full model without the sting are also presented. Further, a few results for the 'shelf' configuration under Mach 4.5 flight conditions in equilibrium Mars gas as well as in a perfect gas with an effective γ are also presented.

The Baseline Configuration:

The results for the baseline configuration are listed in Table 2, and are shown plotted in Figure 5 for Mach 2.3, 2.7, 3.5, and 4.5. These computations were done for only the forebody; the aftbody was absent in the computational model. It may be observed from Figures 5 that C_m, L/D, and C_N vary linearly with α, and do not depend on the Mach number, except at $\alpha = 20$ degrees. Both C_A and C_D are maximum at $\alpha = 0$ degrees, and decreases with increasing angle of attack. With increase in Mach number, these values increase. As the Mach number increases, the forebody surface pressures increase which result in increased C_A. The drag coefficient, C_D, which is essentially a component of C_A, varies similar to C_A. The magnitudes of C_N are small compared to the magnitudes of C_A.

Figures 6 to 9 show comparisons of the present results with the tunnel data for Mach numbers 2.3, 2.7, 3.5, and 4.5, respectively. As noted before, the wind tunnel model was a full model, and had a sting at the base to support the model in the wind tunnel test section. Most of the present computations, however, were

done on the forebody only, and the aftbody was absent (see Figure 2). This would lead to differences in the test data and CFD results in those cases where the pressures acting on the aftbody contributed significantly to the loads. An examination of the figures 6–9 shows that the computed C_m agrees with the test data at Mach 2.3. At higher Mach numbers there are small differences between the two; the computed points lie above the test data. Computed L/D values agree with the test data for all Mach numbers and angles of attack except at $\alpha = 20$ degrees. The computed values of C_A are smaller than the measured values by about 0.16 at Mach 2.3. This difference decreases with increase in Mach number, and at Mach 4.5 the difference is 0.03 which is about 2%. The wind tunnel C_N vs. α curves exhibit a peculiar trend at low angles of attack. At $\alpha = 0$, the curve has a negative slope, and the C_N values are negative between 0 and 2 degrees, This trend is very prominent at Mach 2.3, and disappears gradually as the freestream Mach numbers increases to 4.5. A similar trend had been observed in the past during tests on a similar model (see [7]). The exact cause of this is not been fully understood. Also, at angles of attack greater than 12 degrees, C_N increases rapidly. The present computations do not show any of this trend.

Figure 10 shows the C_p contours on the symmetry plane for Mach 4.5 and $\alpha = 8$, 12, 16, and 20 degrees. Figure 11 presents C_p contours on the symmetry plane for $\alpha = 15$ degrees and Mach 2.3, 3.5, and 4.5.

Wind Tunnel Model Configuration:

In an attempt to reproduce the conditions in the wind tunnel, computations were done for the baseline body in the wind tunnel model configuration (full model with a support sting) as shown in Figure 3. These computations were done for Mach 2.3 at α = -4 to 20, and for Mach 4.5 at $\alpha = 0$ to 5 degrees. The results are also shown in Figures 6 & 9. It may be noticed that C_m and L/D do not change from the forebody values at Mach 2.3 and 4.5. The agreement between the computed C_A as well as C_D and the wind tunnel data is much better at Mach 2.3. The C_N exhibits a non-linear trend with angle of attack. However, the trend noticed in the wind tunnel data at low angles of attack is not seen in the results for Mach 2.3. At $\alpha = 12$ degrees and higher, the computed results agree very well with the wind tunnel data.

Examination of the flow over the body and the symmetry plane shows what appears to be a separated flow on the aftbody (see Figures 12 to 14). It should be recalled here that the present computations are inviscid, and the boundary layer is absent. Nevertheless, the numerical viscosity in the solution algorithm causes the flow to "separate" similar to what happens in viscous flow. Figure 12–14 shows the streamlines on the body as well as on the symmetry plane for Mach 2.3, and $\alpha = 0$, 5, 8, 12, 16, and 20 degrees. The separated flow region for low angles of attack is nearly symmetric about the longitudinal axis. The pressures on the aftbody contribute not only to C_A but also to C_N. This is evident in the C_N vs. α curve for Mach 2.3. For α greater than 8 degrees, there is a marked asymmetry in the separated flow region. The resulting pressure distribution on the aftbody gives rise to a normal force. The computed values of C_N for α greater than 10 degrees agree very well with the tunnel data. The differences between the computational results for forebody and full model are small (0.02 at $\alpha = 20$ degrees), and do not seem to contribute to the pitching moment.

The Shelf configuration:

The results for the 'shelf' configuration are shown plotted in Figure 15 for Mach 2.3, 2.7, 3.5, and 4.5. The variations of the aerodynamic coefficients with angle of attack and Mach number in general are very similar to what was observed for the baseline configuration. The pitching moment varies linearly with angle of attack for the four Mach numbers. The curves shift upwards as the Mach number is increased from 2.3 to 4.5. The

trim angles of attack are 13.1 degrees for Mach 2.3 and 14.3 degrees for Mach 4.5. The corresponding L/D values are -0.22 for Mach 2.3 and -0.24 for Mach 4.5

These results are also shown compared with the wind tunnel data. See Figures 16 to 19 The computed C_m values are consistently below the wind tunnel data, and the two curves are nearly parallel to each other at Mach 2.3 and 2.7. At higher Mach numbers, the computations come closer to the test data. The differences between the computed and the tunnel data are larger (0.003) at Mach 2.3, and nearly zero at Mach 4.5. The computed L/D values agree with tunnel data well for all angles of attack at the four Mach numbers. The trend of C_A, C_D, C_N, and C_L for this configuration are similar to that observed for the baseline configuration.

Figure 20 shows the sonic lines for α = -4 to 20 degrees, and Mach 2.3, 3.5, and 4.5.

Wind Tunnel Model Configuration; $\gamma = 1.4$:

Four additional computations were done for the 'shelf' configuration in the wind tunnel model configuration and $\gamma = 1.4$ at Mach 4.5 and α = 8, 12, 16, and 20 degrees. The purpose of these computations was to check how well the full model computations predict the aerodynamic data for the full model at Mach 4.5. The results of these computations are listed in Table 5, and also shown in Figure 21. The agreement between these results and the wind tunnel test data is much better than the forebody alone. The axial force coefficients differ by less than 0.02 at α = 8 degrees, and this difference decreases to zero at α = 20 degrees. The steep rise in the normal force coefficient beyond $\alpha > 12$ degrees is also predicted by the computations. It may be recalled that a similar comparison was noted for the baseline configurations for Mach 2.3.

Computations with Mars Gas and an effective γ:

Two additional computations were done for the 'shelf' forebody with equilibrium Mars gas with flight conditions for Mach 4.5. The freestream conditions are as follows:

Velocity	967.6 m/s
Density	2.183E-03 kg/m^3
Temperature	184.4 K

Further, two more computations were done with $\gamma = 1.24$ to see how well the results of computations with an effective γ compare with the Mars gas. The effective γ is defined as the value of isentropic index that produces a normal-shock-density-ratio equal to that for the equilibrium Mars gas. This value depends on the freestream conditions; for Mach 4.5 flight conditions the value is 1.24. The results of these computations are listed in Table 5 and shown graphically in Figure 22. An examination of this figure shows that the Mars gas and $\gamma = 1.24$ produce results that are almost indistinguishable from each other. Further a comparison of these results with the results for $\gamma = 1.4$ show differences in C_m and C_A. There is an increase in C_m and also in C_A. The increased C_m would increase the trim angle by about 2 degrees. The increase in C_A (and consequently C_D) is 0.06 at α = 10 degrees. The C_N does not seem to be affected noticeably.

Computations were done on the full model with and without the support sting to study the effect of the aftbody on the results with $\gamma = 1.24$. Results of these computations are also listed in Table 5 and are shown in Figure 22. The effect of the aftbody is seen primarily in C_A, C_D, and in C_N. The pressures on the aftbody do not seem to affect the C_m. Both axial and normal force coefficients increases due to the aftbody; changes in C_D are similar to those in C_A. The normal force coefficient seems to rise steeply with increase in α. These are consistent with the observation made on the baseline configuration. Also, the presence of the sting on the aerodynamic coefficients under these conditions (M = 4.5, $\gamma = 1.24$) is negligible.

The 'canted' and the 'Ames' configurations:

The results for the 'canted' and 'Ames' configurations are shown plotted in Figure 23 & 28. These results are also shown compared with the wind tunnel test data Figures 24 to 27 and 29 to 31. It may be seen in these figures that the trends in all the aerodynamic coefficients at the four Mach numbers is similar to what was seen for the 'shelf' configuration. The 'canted' body behaves very similar to the 'shelf'. The 'Ames' body has a larger tab, and hence trims at a 17 angle of attack, and produces a trim L/D of -0.28 at M=4.5.

Conclusion

Inviscid longitudinal aerodynamic characteristics of the three aeroshell configuration for the proposed '07 Mars lander are presented. These shapes are designated the 'shelf', the 'canted', and the 'Ames'. Aerodynamic data for the baseline configuration are also computed, and are included in this report. The results are for Mach 2.3, 2.7, 3.5, and 4.5, and for α from -4 to +20 degrees. These results are compared with the data from model tests in the NASA Unitary Plan Wind Tunnel. The comparison showed that computed aerodynamic coefficients compare well with wind tunnel data at Mach 4.5. At lower Mach numbers the comparison is not as good, particularly in C_A and C_N. The differences between the computed and wind tunnel data are attributed to the pressures acting on the aft part of these bodies. Most of the present computations were done on the forebody only; the aftbody was absent in these computational models. A few computations done for computational models with the aftbody and sting show that, at lower Mach numbers, the aftbody pressure contribute significantly to C_A and C_N. The aftbody pressures account for most of the differences between the wind tunnel data and the (forebody only) axial force coefficients. The pitching moment coefficient is not affected noticeably by the aftbody pressures. This study also indicated that flow "separation" on the aftbody at angles of attack greater than 8 degrees leads to nonlinear trends in C_N with α.

A few computations were done at Mach 4.5 in Mars gas environment as well as with an effective γ. There was a very good agreement between these two sets of results, indicating that, at these low Mach numbers, the computations with an effective γ yield results that are nearly the same as would be found in Mars gas.

Acknowledgments

The work described herein was performed at Lockheed Martin Engineering & Sciences Company in Hampton, Virginia, and was supported by Aerothermodynamics Branch, NASA Langley Research Center under the contract NAS1-00135. The technical monitor was Dr. Kenneth Sutton. The tunnel data in the form of curve fits were provided by Ms. Kelly Murphy of the Aerothermodynamics Branch.

References

[1] Lockwood, M.K., Powell, R.W., Graves, S.G., and Carman, G.L.: "Entry System Design Considerations for Mars Landers," AAS 01-023, 24th Annual AAS Guidance and Control Conference, January–February, 2001.

[2] Prabhu, R.K.: "Inviscid Flow Computations of Several Aeroshell Configurations for a '07 Mars Lander," NASA/CR-2001-210851, April 2001.

[3] Prabhu, R.K.: "Inviscid Flow Computations of Two '07 Mars Lander Aeroshell Configurations Over a Mach Number Range of 2 to 24," NASA/CR-2001-210852, April 2001.

[4] Peiro, J., Peraire, J., and Morgan, K.: "FELISA System Reference Manual and User's Guide," Technical Report, University College, Swansea, Wales, 1993, (Also NASA CP 3291, May 1995.)

[5] Bibb, K.L., Peraire, J., and Riley, C.J.: "Hypersonic Flow Computation on Unstructured Meshes," AIAA Paper 97-0625, January 1997.

[6] Samereh, J.: "GridTool: A Surface Modeling and Grid Generation Tool," NASA CP 3291, May 1995.

[7] Blake, W.W.: "Experimental Aerodynamic Characteristics of the Viking Entry Vehicle Over the Mach Number Range 1.5–10," Martin Marietta Contractor Report TR-372106, April 1971.

Mach No.	α, deg.	C_N	C_A	C_m	C_L	C_D	L/D
2.3	-4.0	-9.9624E-03	1.3743	7.3799E-03	8.5928E-02	1.3716	6.2646E-02
2.3	0.0	-2.1217E-04	1.3782	5.1236E-05	-2.1217E-04	1.3782	-1.5395E-04
2.3	4.0	9.5892E-03	1.3743	-7.2949E-03	-8.6300E-02	1.3716	-6.2919E-02
2.3	8.0	1.9304E-02	1.3626	-1.4550E-02	-1.7052E-01	1.3520	-1.2612E-01
2.3	12.0	2.8956E-02	1.3428	-2.1710E-02	-2.5086E-01	1.3195	-1.9012E-01
2.3	16.0	3.8496E-02	1.3145	-2.8710E-02	-3.2532E-01	1.2742	-2.5532E-01
2.3	20.0	4.7998E-02	1.2768	-3.5574E-02	-3.9159E-01	1.2162	-3.2197E-01
2.7	-4.0	-1.0074E-02	1.4150	7.4349E-03	8.8656E-02	1.4123	6.2776E-02
2.7	0.0	-1.8801E-04	1.4191	4.4844E-05	-1.8801E-04	1.4191	-1.3249E-04
2.7	4.0	9.6443E-03	1.4150	-7.3095E-03	-8.9085E-02	1.4122	-6.3081E-02
2.7	8.0	1.9471E-02	1.4026	-1.4629E-02	-1.7592E-01	1.3917	-1.2641E-01
2.7	12.0	2.9187E-02	1.3813	-2.1809E-02	-2.5864E-01	1.3572	-1.9057E-01
2.7	16.0	3.8827E-02	1.3506	-2.8842E-02	-3.3495E-01	1.3090	-2.5589E-01
2.7	20.0	4.8565E-02	1.3091	-3.5818E-02	-4.0210E-01	1.2468	-3.2252E-01
3.5	-4.0	-1.0094E-02	1.4612	7.4142E-03	9.1859E-02	1.4583	6.2988E-02
3.5	0.0	-1.7304E-04	1.4656	3.1700E-05	-1.7304E-04	1.4656	-1.1807E-04
3.5	4.0	9.7103E-03	1.4612	-7.3231E-03	-9.2242E-02	1.4583	-6.3252E-02
3.5	8.0	1.9542E-02	1.4476	-1.4605E-02	-1.8212E-01	1.4362	-1.2680E-01
3.5	12.0	2.9351E-02	1.4242	-2.1791E-02	-2.6740E-01	1.3992	-1.9111E-01
3.5	16.0	3.9205E-02	1.3897	-2.8894E-02	-3.4537E-01	1.3467	-2.5646E-01
3.5	20.0	4.9530E-02	1.3415	-3.6186E-02	-4.1228E-01	1.2775	-3.2271E-01
4.5	-4.0	-1.0096E-02	1.4894	7.3686E-03	9.3824E-02	1.4865	6.3118E-02
4.5	0.0	-1.8435E-04	1.4941	3.2561E-05	-1.8435E-04	1.4941	-1.2339E-04
4.5	4.0	9.7301E-03	1.4895	-7.3010E-03	-9.4196E-02	1.4866	-6.3365E-02
4.5	8.0	1.9527E-02	1.4751	-1.4510E-02	-1.8596E-01	1.4635	-1.2707E-01
4.5	12.0	2.9340E-02	1.4500	-2.1620E-02	-2.7277E-01	1.4244	-1.9150E-01
4.5	16.0	3.9389E-02	1.4121	-2.8792E-02	-3.5136E-01	1.3683	-2.5680E-01
4.5	20.0	5.0618E-02	1.3574	-3.6641E-02	-4.1669E-01	1.2929	-3.2231E-01

Table 2: Summary of aerodynamic coefficients for 'baseline' forebody.

Mach No.	α, deg.	C_N	C_A	C_m	C_L	C_D	L/D
2.3	0.0	-2.1035E-04	1.5584	-2.1060E-05	-2.1035E-04	1.5584	-1.3498E-04
2.3	1.0	3.1944E-03	1.5582	-1.9248E-03	-2.4000E-02	1.5580	-1.5404E-02
2.3	2.0	5.6125E-03	1.5580	-3.9234E-03	-4.8764E-02	1.5572	-3.1314E-02
2.3	3.0	8.7543E-03	1.5571	-5.8740E-03	-7.2750E-02	1.5554	-4.6772E-02
2.3	4.0	1.2411E-02	1.5562	-7.8081E-03	-9.6174E-02	1.5533	-6.1917E-02
2.3	5.0	1.6191E-02	1.5544	-9.7277E-03	-1.1935E-01	1.5499	-7.7002E-02
2.3	8.0	2.5503E-02	1.5459	-1.5446E-02	-1.8989E-01	1.5344	-1.2376E-01
2.3	12.0	2.8358E-02	1.5374	-2.2170E-02	-2.9191E-01	1.5097	-1.9335E-01
2.3	16.0	4.6564E-02	1.5116	-2.9373E-02	-3.7189E-01	1.4659	-2.5370E-01
2.3	20.0	6.9515E-02	1.4755	-3.6283E-02	-4.3933E-01	1.4103	-3.1152E-01
4.5	0.0	-2.5092E-04	1.5276	6.1677E-06	-2.5092E-04	1.5276	-1.6426E-04
4.5	1.0	2.7317E-03	1.5273	-1.9026E-03	-2.3924E-02	1.5271	-1.5666E-02
4.5	2.0	5.6031E-03	1.5266	-3.8278E-03	-4.7678E-02	1.5259	-3.1246E-02
4.5	3.0	8.5654E-03	1.5254	-5.7405E-03	-7.1280E-02	1.5238	-4.6779E-02
4.5	4.0	1.1813E-02	1.5236	-7.6431E-03	-9.4497E-02	1.5207	-6.2140E-02
4.5	5.0	1.4996E-02	1.5210	-9.5442E-03	-1.1762E-01	1.5165	-7.7562E-02

Table 3: Summary of aerodynamic coefficients for 'baseline' full model configuration.

Mach No.	α, deg.	C_N	C_A	C_m	C_L	C_D	L/D
2.3	-4.0	-3.0764E-02	1.4358	3.6454E-02	6.9467E-02	1.4344	4.8428E-02
2.3	0.0	-2.0239E-02	1.4387	2.8035E-02	-2.0239E-02	1.4387	-1.4068E-02
2.3	4.0	-9.5881E-03	1.4332	1.9514E-02	-1.0954E-01	1.4290	-7.6653E-02
2.3	8.0	1.1545E-03	1.4192	1.0945E-02	-1.9637E-01	1.4055	-1.3971E-01
2.3	12.0	1.1964E-02	1.3964	2.3462E-03	-2.7863E-01	1.3684	-2.0362E-01
2.3	16.0	2.2839E-02	1.3645	-6.2407E-03	-3.5415E-01	1.3179	-2.6872E-01
2.3	20.0	3.3705E-02	1.3228	-1.4728E-02	-4.2075E-01	1.2546	-3.3538E-01
2.7	-4.0	-3.1640E-02	1.4782	3.7328E-02	7.1551E-02	1.4768	4.8450E-02
2.7	0.0	-2.1078E-02	1.4813	2.8907E-02	-2.1078E-02	1.4813	-1.4229E-02
2.7	4.0	-1.0359E-02	1.4755	2.0363E-02	-1.1326E-01	1.4712	-7.6985E-02
2.7	8.0	5.1076E-04	1.4606	1.1721E-02	-2.0277E-01	1.4465	-1.4018E-01
2.7	12.0	1.1418E-02	1.4363	3.0888E-03	-2.8746E-01	1.4073	-2.0426E-01
2.7	16.0	2.2375E-02	1.4021	-5.4999E-03	-3.6496E-01	1.3540	-2.6955E-01
2.7	20.0	3.3510E-02	1.3563	-1.4122E-02	-4.3239E-01	1.2860	-3.3624E-01
3.5	-4.0	-3.2626E-02	1.5262	3.8322E-02	7.3916E-02	1.5248	4.8477E-02
3.5	0.0	-2.2010E-02	1.5296	2.9907E-02	-2.2010E-02	1.5296	-1.4389E-02
3.5	4.0	-1.1188E-02	1.5233	2.1322E-02	-1.1742E-01	1.5188	-7.7311E-02
3.5	8.0	-2.5775E-04	1.5072	1.2703E-02	-2.1002E-01	1.4925	-1.4072E-01
3.5	12.0	1.0771E-02	1.4805	4.0289E-03	-2.9728E-01	1.4504	-2.0496E-01
3.5	16.0	2.1975E-02	1.4421	-4.6743E-03	-3.7637E-01	1.3923	-2.7033E-01
3.5	20.0	3.3764E-02	1.3895	-1.3667E-02	-4.4351E-01	1.3173	-3.3669E-01
4.5	-4.0	-3.3176E-02	1.5556	3.8892E-02	7.5418E-02	1.5541	4.8528E-02
4.5	0.0	-2.2539E-02	1.5593	3.0518E-02	-2.2539E-02	1.5593	-1.4455E-02
4.5	4.0	-1.1726E-02	1.5527	2.1982E-02	-1.2001E-01	1.5481	-7.7520E-02
4.5	8.0	-8.3281E-04	1.5356	1.3426E-02	-2.1454E-01	1.5205	-1.4109E-01
4.5	12.0	1.0232E-02	1.5071	4.8315E-03	-3.0334E-01	1.4763	-2.0547E-01
4.5	16.0	2.1627E-02	1.4652	-3.9038E-03	-3.8307E-01	1.4144	-2.7084E-01
4.5	20.0	3.4397E-02	1.4059	-1.3585E-02	-4.4852E-01	1.3329	-3.3651E-01

Table 4: Summary of aerodynamic coefficients for 'shelf' forebody.

Gas Model	**Mach No.**	α **deg.**	C_N	C_A	C_m	C_L	C_D	L/D	**Config.**
γ=1.4	4.5	8.0	-3.304E-03	1.5789	1.363E-02	-2.230E-01	1.5631	-1.4268-01	Body+Sting
γ=1.4	4.5	12.0	1.321E-02	1.5515	5.190E-03	-3.096E-01	1.5203	-2.037E-01	Body+Sting
γ=1.4	4.5	16.0	3.158E-02	1.5092	-3.519E-03	-3.856E-01	1.4594	-2.642E-01	Body+Sting
γ=1.4	4.5	20.0	5.286E-02	1.4481	-1.312E-02	-4.456E-01	1.3788	-3.232E-01	Body+Sting
γ=1.24	4.5	10.0	3.213E-03	1.5895	1.202E-02	-2.729E-01	1.5659	-1.742E-01	Forebody
γ=1.24	4.5	14.0	1.497E-02	1.5459	3.449E-03	-3.595E-01	1.5036	-2.391E-01	Forebody
Mars Gas	4.5	10.0	2.966E-03	1.5888	1.214E-02	-2.730E-01	1.5652	-1.744E-01	Forebody
Mars Gas	4.5	14.0	1.421E-02	1.5477	4.006E-03	-3.606E-01	1.5052	-2.396E-01	Forebody
γ=1.24	4.5	10.0	7.313E-03	1.6362	1.244E-02	-2.769E-01	1.6126	-1.717E-01	Body+Sting
γ=1.24	4.5	14.0	2.713E-02	1.5930	4.342E-03	-3.591E-01	1.5522	-2.313E-01	Body+Sting
γ=1.24	4.5	10.0	8.283E-03	1.6418	1.282E-02	-2.769E-01	1.6183	-1.711E-01	Body, No Sting
γ=1.24	4.5	14.0	2.717E-02	1.5975	4.507E-03	-3.601E-01	1.5566	-2.313E-01	Body, No Sting

Table 5: Summary of aerodynamic coefficients for 'shelf', flight conditions.

Mach No.	α, deg.	C_N	C_A	C_m	C_L	C_D	L/D
2.3	-4.0	-1.9757E-02	1.4228	3.0188E-02	7.9541E-02	1.4207	5.5986E-02
2.3	0.0	-1.0144E-02	1.4273	2.2479E-02	-1.0144E-02	1.4273	-7.1071E-03
2.3	4.0	-4.5003E-04	1.4236	1.4745E-02	-9.9754E-02	1.4201	-7.0244E-02
2.3	8.0	9.2349E-03	1.4117	7.0185E-03	-1.8733E-01	1.3992	-1.3388E-01
2.3	12.0	1.8938E-02	1.3915	-6.4701E-04	-2.7078E-01	1.3650	-1.9837E-01
2.3	16.0	2.8555E-02	1.3623	-8.1480E-03	-3.4805E-01	1.3174	-2.6420E-01
2.3	20.0	3.8130E-02	1.3237	-1.5485E-02	-4.1690E-01	1.2569	-3.3169E-01
2.7	-4.0	-2.0062E-02	1.4645	3.0924E-02	8.2145E-02	1.4623	5.6174E-02
2.7	0.0	-1.0406E-02	1.4693	2.3223E-02	-1.0406E-02	1.4693	-7.0823E-03
2.7	4.0	-6.6418E-04	1.4655	1.5467E-02	-1.0289E-01	1.4619	-7.0382E-02
2.7	8.0	9.0764E-03	1.4530	7.7716E-03	-1.9323E-01	1.4401	-1.3418E-01
2.7	12.0	1.8806E-02	1.4313	1.5063E-04	-2.7919E-01	1.4039	-1.9886E-01
2.7	16.0	2.8501E-02	1.3998	-7.3465E-03	-3.5844E-01	1.3534	-2.6484E-01
2.7	20.0	3.8326E-02	1.3572	-1.4756E-02	-4.2818E-01	1.2885	-3.3232E-01
3.5	-4.0	-2.0385E-02	1.5121	3.1754E-02	8.5143E-02	1.5098	5.6392E-02
3.5	0.0	-1.0694E-02	1.5173	2.4069E-02	-1.0694E-02	1.5173	-7.0480E-03
3.5	4.0	-9.3172E-04	1.5132	1.6373E-02	-1.0648E-01	1.5094	-7.0546E-02
3.5	8.0	8.8554E-03	1.4997	8.7310E-03	-1.9995E-01	1.4863	-1.3452E-01
3.5	12.0	1.8620E-02	1.4760	1.1970E-03	-2.8866E-01	1.4476	-1.9941E-01
3.5	16.0	2.8494E-02	1.4407	-6.2665E-03	-3.6972E-01	1.3927	-2.6546E-01
3.5	20.0	3.8968E-02	1.3908	-1.3961E-02	-4.3906E-01	1.3203	-3.3256E-01
4.5	-4.0	-2.0527E-02	1.5412	3.2182E-02	8.7032E-02	1.5389	5.6555E-02
4.5	0.0	-1.0875E-02	1.5468	2.4612E-02	-1.0875E-02	1.5468	-7.0306E-03
4.5	4.0	-1.1375E-03	1.5426	1.6999E-02	-1.0874E-01	1.5388	-7.0668E-02
4.5	8.0	8.5640E-03	1.5284	9.5159E-03	-2.0423E-01	1.5147	-1.3483E-01
4.5	12.0	1.8293E-02	1.5032	2.1760E-03	-2.9464E-01	1.4742	-1.9987E-01
4.5	16.0	2.8305E-02	1.4646	-5.1801E-03	-3.7649E-01	1.4157	-2.6595E-01
4.5	20.0	4.0012E-02	1.4072	-1.3724E-02	-4.4369E-01	1.3360	-3.3210E-01

Table 6: Summary of aerodynamic coefficients for 'canted' forebody.

Mach No.	α, deg.	C_N	C_A	C_m	C_L	C_D	L/D
2.3	-4.0	-3.7264E-02	1.4494	4.6583E-02	6.3932E-02	1.4485	4.4138E-02
2.3	0.0	-2.6234E-02	1.4510	3.7411E-02	-2.6234E-02	1.4510	-1.8080E-02
2.3	4.0	-1.4999E-02	1.4439	2.8026E-02	-1.1568E-01	1.4393	-8.0373E-02
2.3	8.0	-3.6459E-03	1.4282	1.8536E-02	-2.0238E-01	1.4138	-1.4314E-01
2.3	12.0	7.7690E-03	1.4036	9.0156E-03	-2.8423E-01	1.3745	-2.0678E-01
2.3	16.0	1.9200E-02	1.3698	-5.1140E-04	-3.5911E-01	1.3220	-2.7164E-01
2.3	20.0	3.0558E-02	1.3265	-9.9064E-03	-4.2497E-01	1.2570	-3.3810E-01
2.7	-4.0	-3.8172E-02	1.4928	4.7903E-02	6.6053E-02	1.4918	4.4277E-02
2.7	0.0	-2.7072E-02	1.4946	3.8698E-02	-2.7072E-02	1.4946	-1.8113E-02
2.7	4.0	-1.5735E-02	1.4871	2.9257E-02	-1.1943E-01	1.4824	-8.0567E-02
2.7	8.0	-4.2594E-03	1.4703	1.9693E-02	-2.0884E-01	1.4554	-1.4350E-01
2.7	12.0	7.2872E-03	1.4441	1.0073E-02	-2.9312E-01	1.4141	-2.0729E-01
2.7	16.0	1.8818E-02	1.4078	5.1821E-04	-3.6995E-01	1.3585	-2.7233E-01
2.7	20.0	3.0366E-02	1.3607	-8.9679E-03	-4.3685E-01	1.2890	-3.3890E-01
3.5	-4.0	-3.9154E-02	1.5418	4.9361E-02	6.8492E-02	1.5408	4.4453E-02
3.5	0.0	-2.7935E-02	1.5438	4.0107E-02	-2.7935E-02	1.5438	-1.8095E-02
3.5	4.0	-1.6496E-02	1.5357	3.0616E-02	-1.2358E-01	1.5308	-8.0729E-02
3.5	8.0	-4.9222E-03	1.5176	2.1006E-02	-2.1608E-01	1.5021	-1.4385E-01
3.5	12.0	6.7047E-03	1.4889	1.1369E-02	-3.0300E-01	1.4578	-2.0785E-01
3.5	16.0	1.8421E-02	1.4489	1.7477E-03	-3.8166E-01	1.3978	-2.7304E-01
3.5	20.0	3.0466E-02	1.3956	-7.9472E-03	-4.4869E-01	1.3219	-3.3944E-01
4.5	-4.0	-3.9719E-02	1.5719	5.0221E-02	7.0028E-02	1.5708	4.4580E-02
4.5	0.0	-2.8516E-02	1.5739	4.0988E-02	-2.8516E-02	1.5739	-1.8118E-02
4.5	4.0	-1.7038E-02	1.5655	3.1521E-02	-1.2620E-01	1.5605	-8.0872E-02
4.5	8.0	-5.4699E-03	1.5464	2.1961E-02	-2.2063E-01	1.5306	-1.4415E-01
4.5	12.0	6.1666E-03	1.5161	1.2411E-02	-3.0918E-01	1.4843	-2.0831E-01
4.5	16.0	1.7998E-02	1.4730	2.8283E-03	-3.8871E-01	1.4209	-2.7357E-01
4.5	20.0	3.0794E-02	1.4136	-7.2737E-03	-4.5454E-01	1.3389	-3.3949E-01

Table 7: Summary of aerodynamic coefficients for 'Ames' forebody.

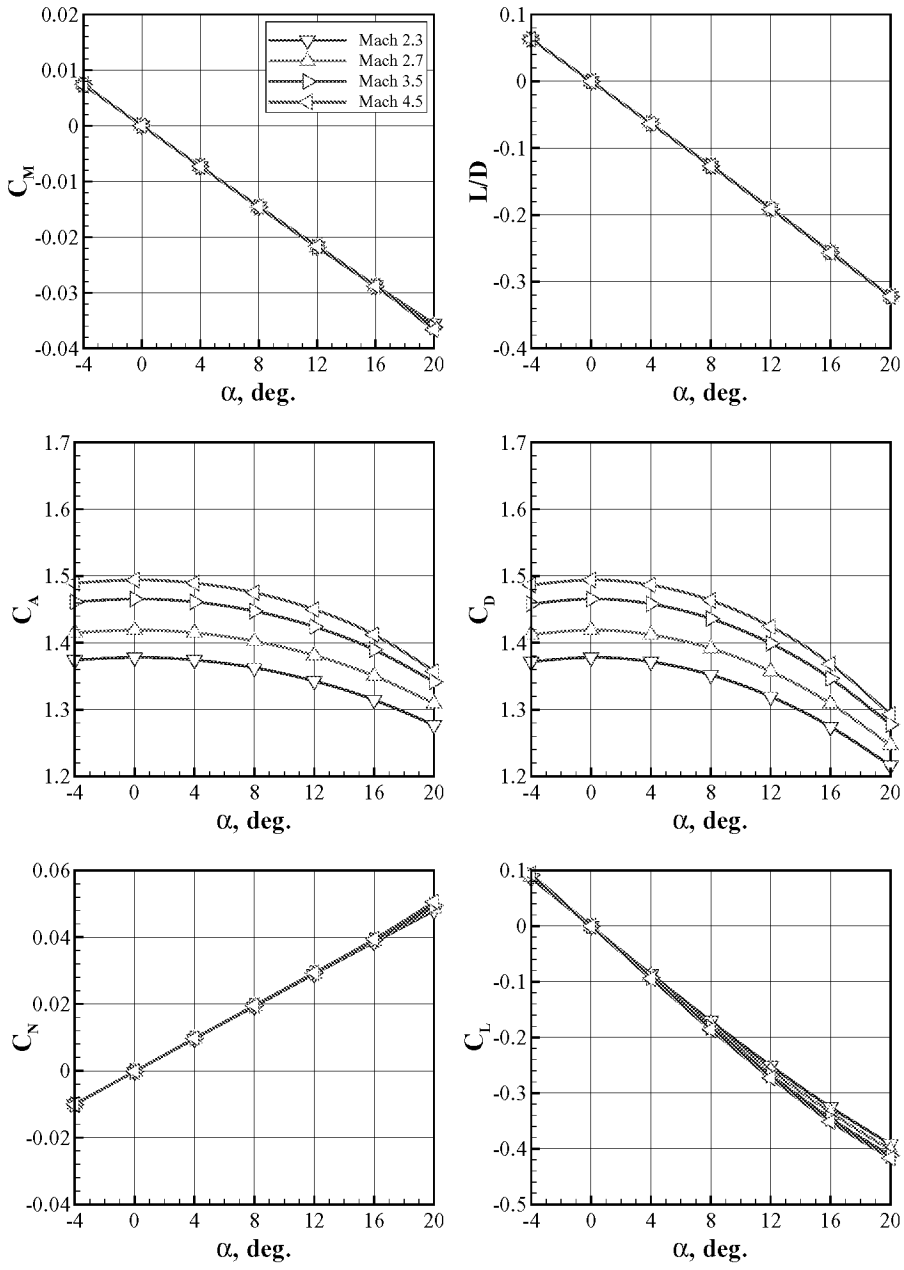

Figure 5: Inviscid aerodynamic data for the baseline forebody.

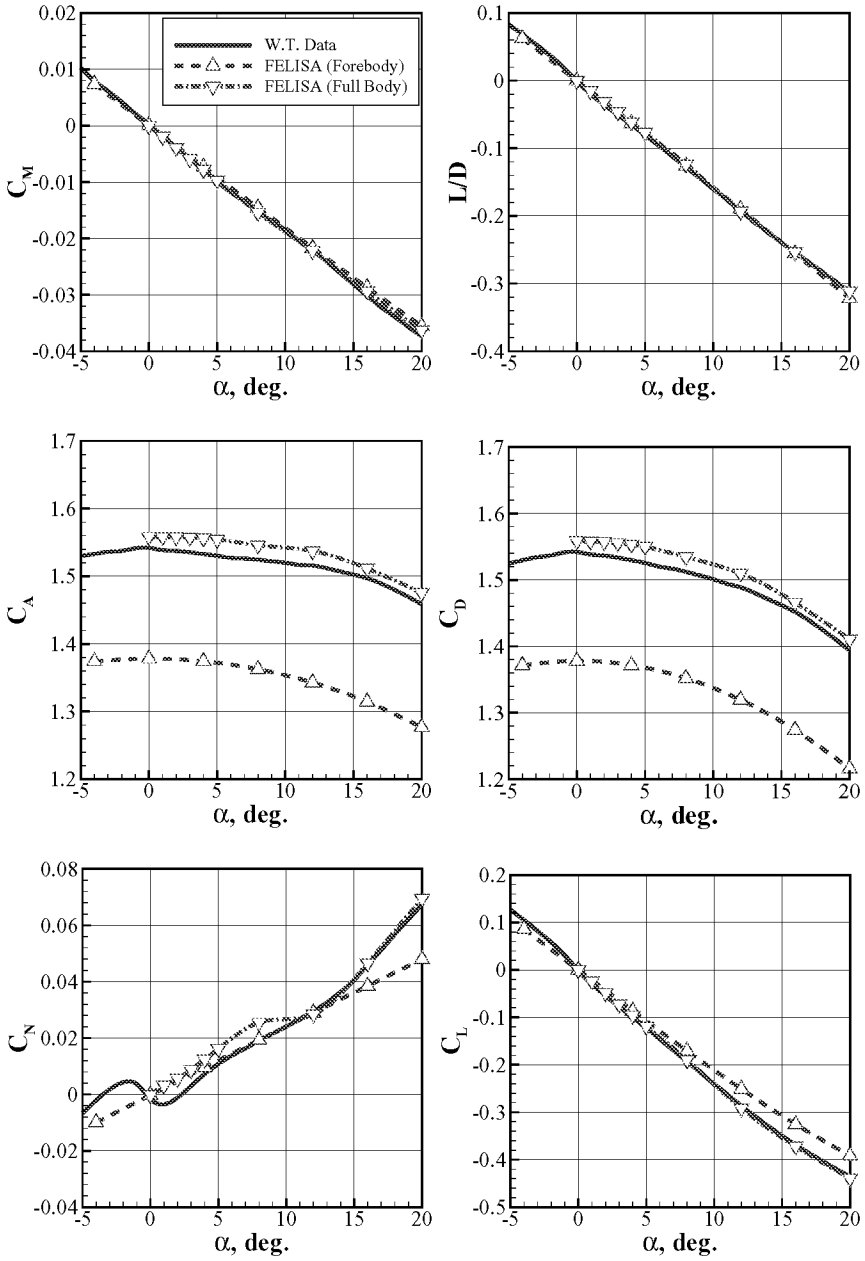

Figure 6: Comparison of CFD and wind tunnel data for the baseline at Mach 2.3.

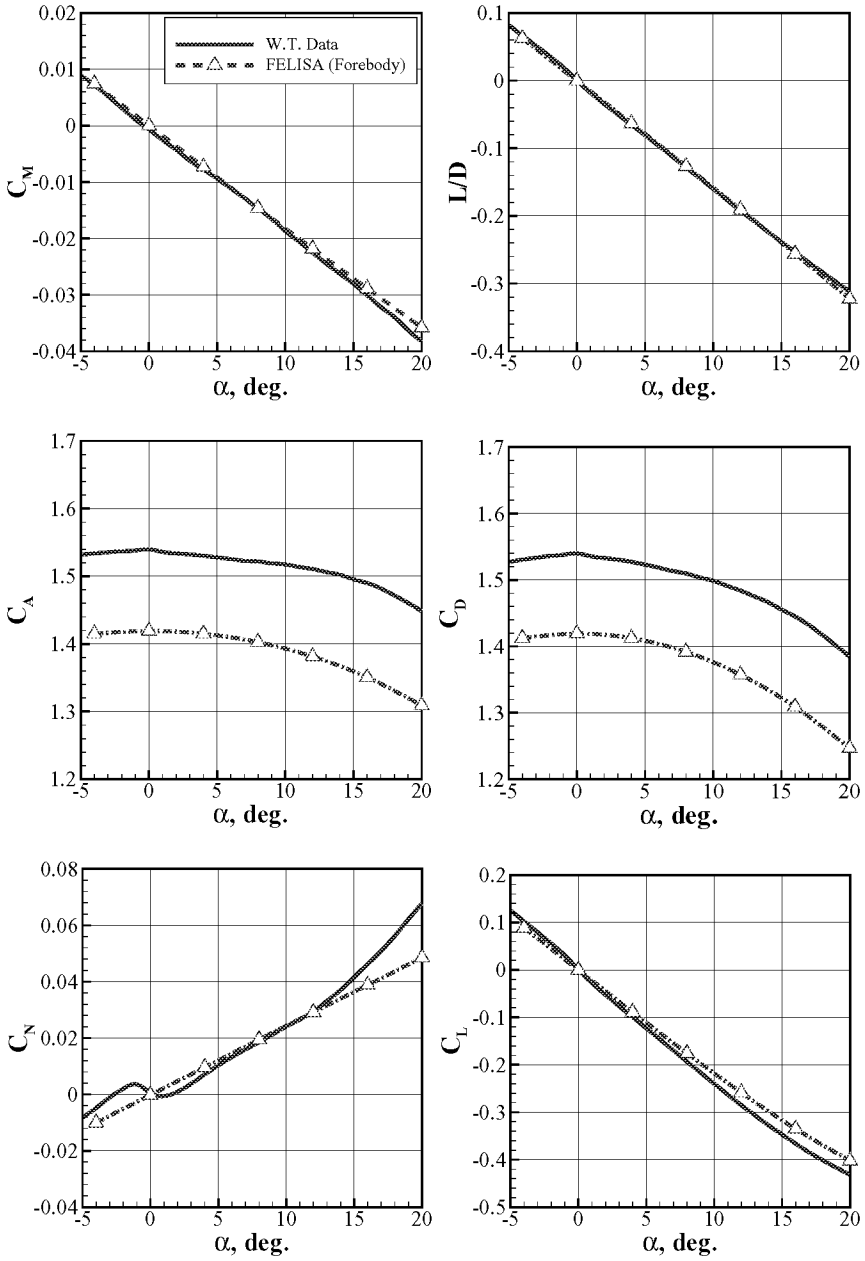

Figure 7: Comparison of CFD and wind tunnel data for the baseline forebody at Mach 2.7.

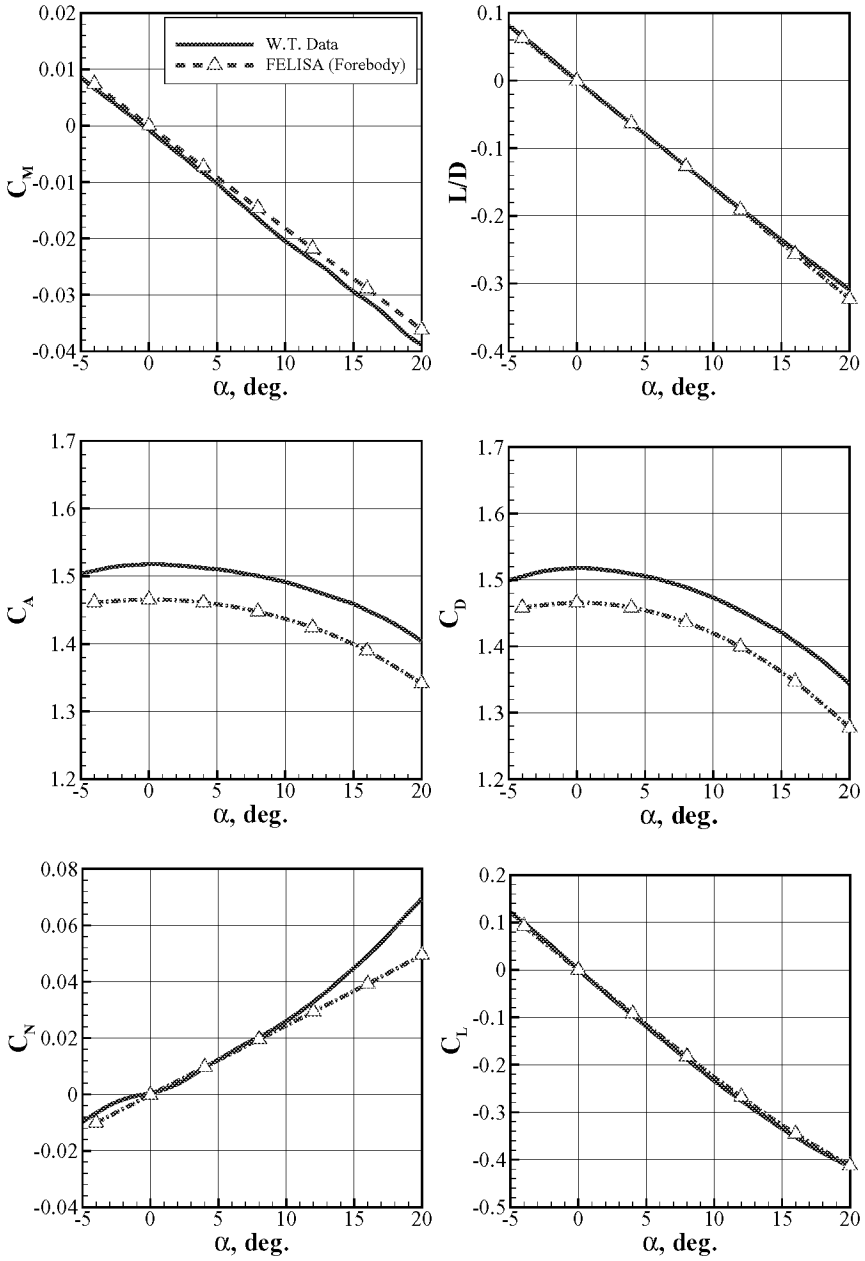

Figure 8: Comparison of CFD and wind tunnel data for the baseline forebody at Mach 3.5.

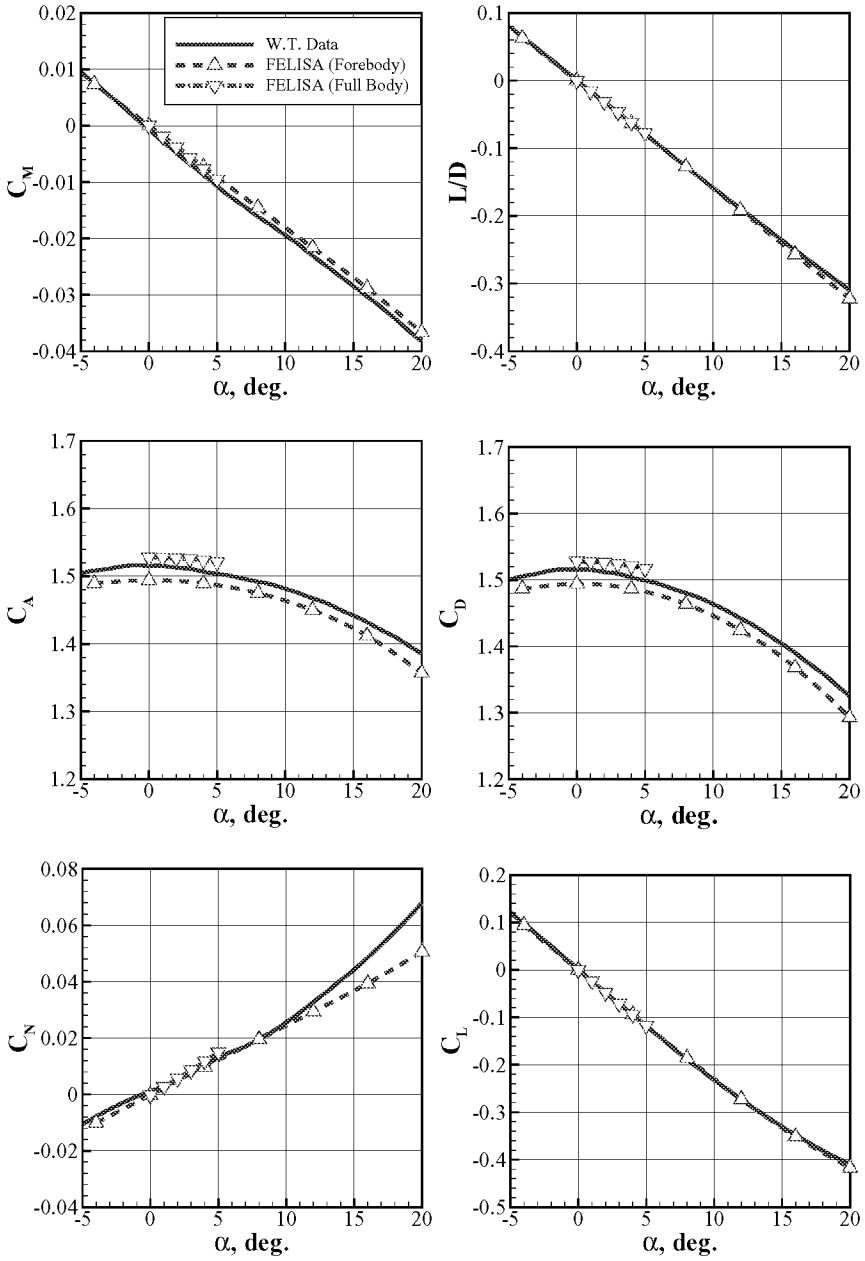

Figure 9: Comparison of CFD and wind tunnel data for the baseline at Mach 4.5.

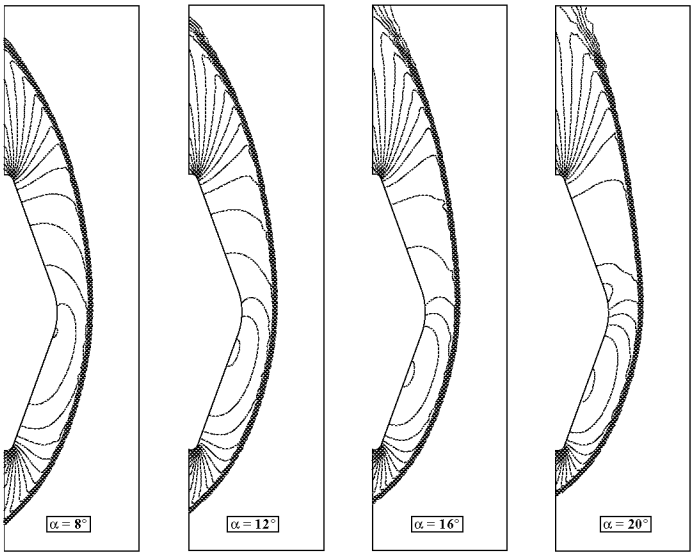

Figure 10: Symmetry plane C_p contours for the baseline at Mach 4.5.

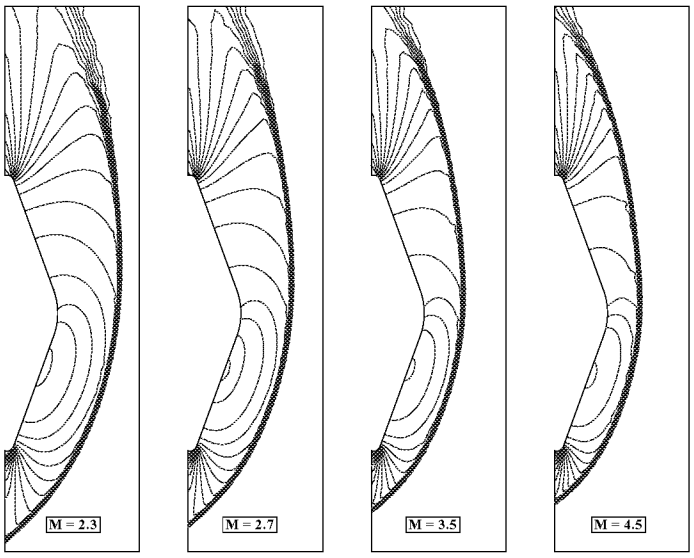

Figure 11: Symmetry plane C_p contours for the baseline at Mach $\alpha = 16$ degrees.

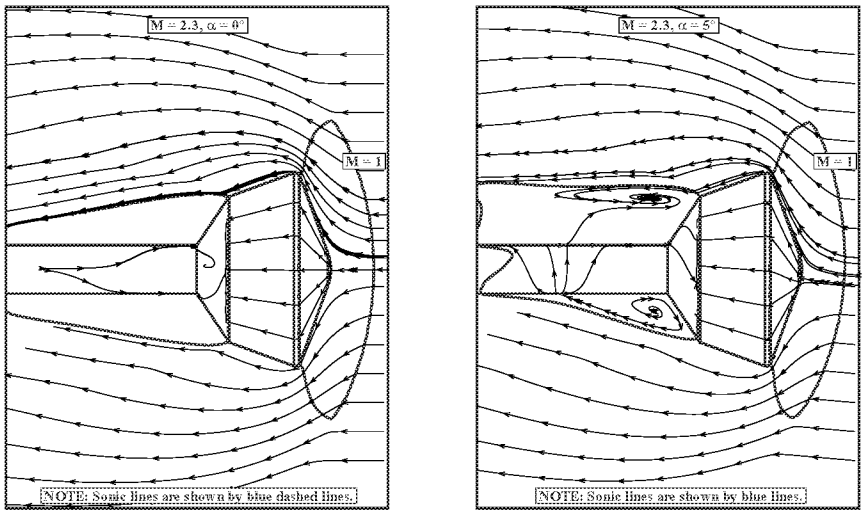

(a) $\alpha = 0°$ (b) $\alpha = 5°$

Figure 12: Streamlines on the body and the symmetry plane for the baseline configuration, M=2.3.

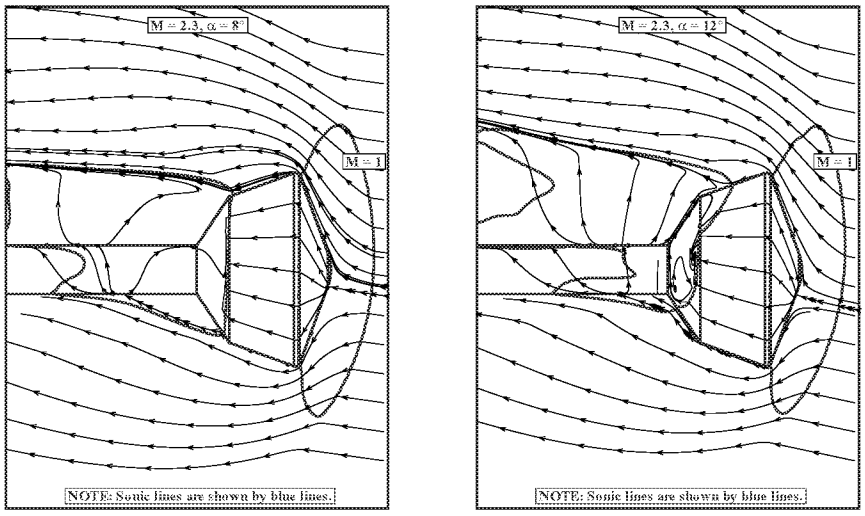

(a) $\alpha = 8°$ (b) $\alpha = 12°$

Figure 13: Streamlines on the body and the symmetry plane for the baseline configuration, M=2.3.

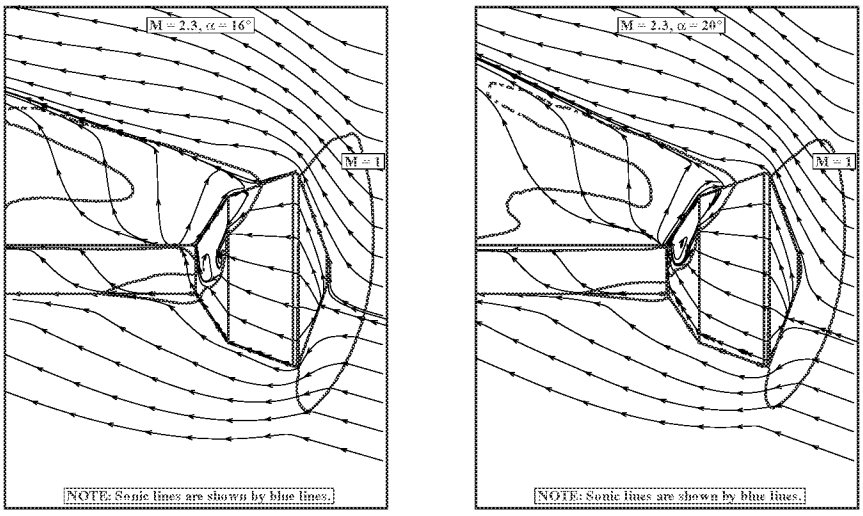

(a) $\alpha = 16°$ (b) $\alpha = 20°$

Figure 14: Streamlines on the body and the symmetry plane for the baseline configuration, M=2.3.

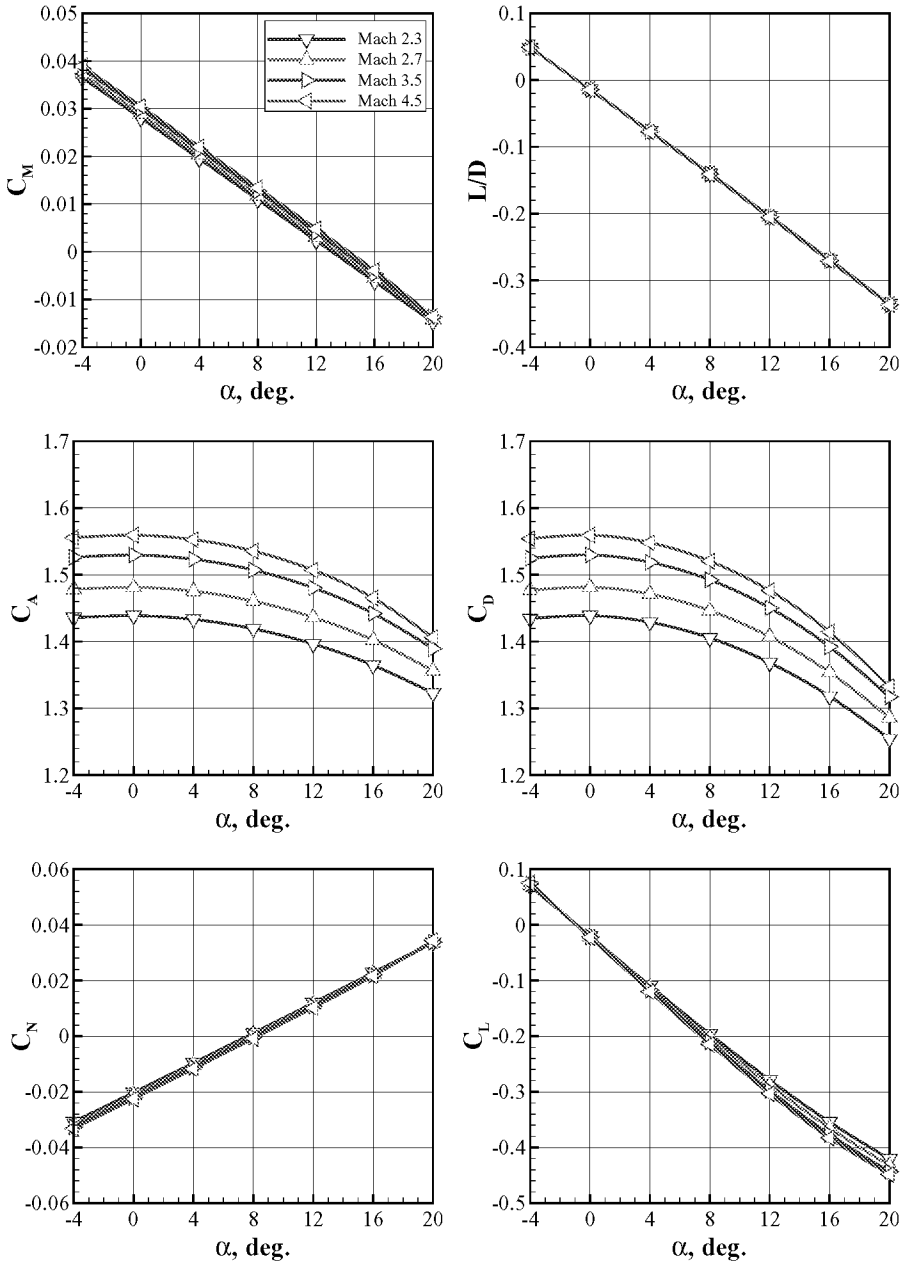

Figure 15: Inviscid aerodynamic data for the 'shelf' forebody.

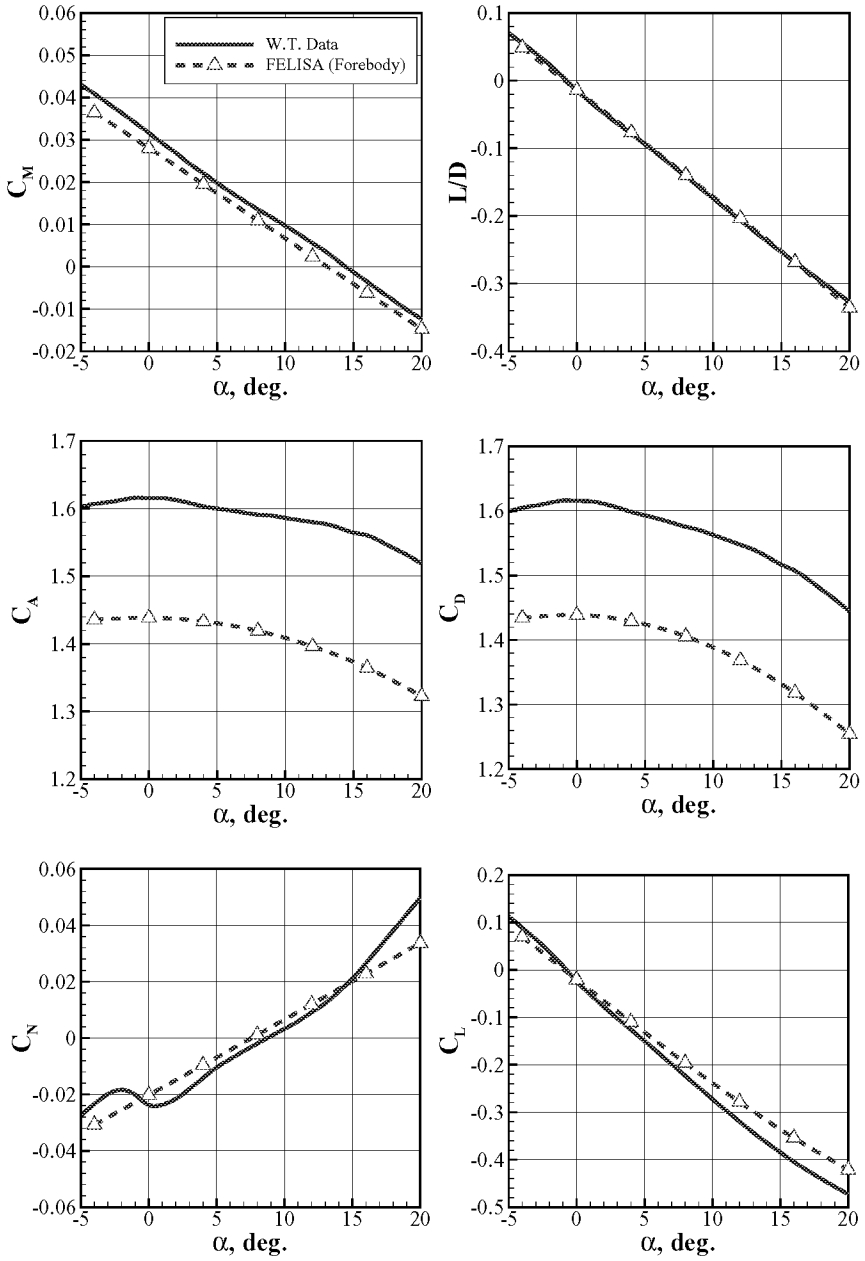

Figure 16: Comparison of aerodynamic data for the 'shelf' configuration at Mach 2.3.

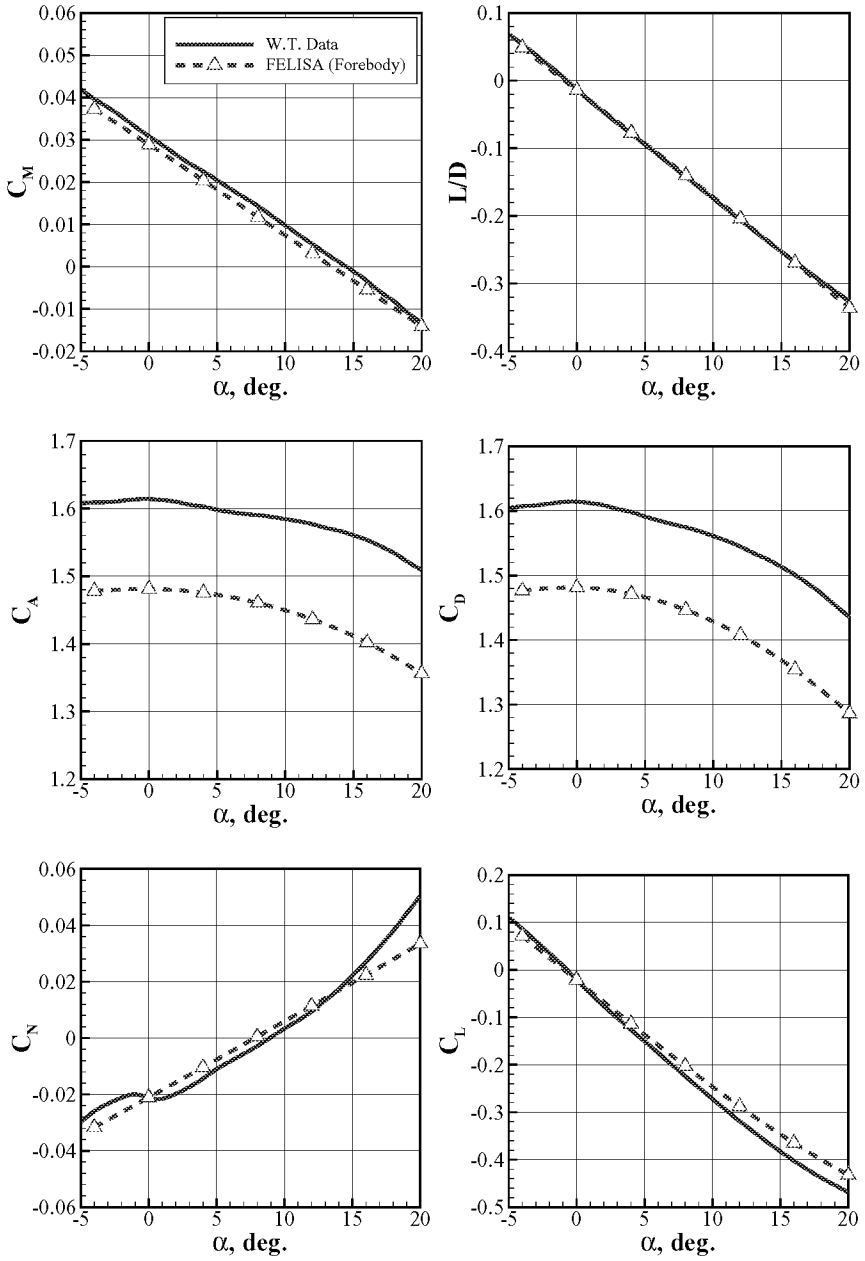

Figure 17: Comparison of aerodynamic data for the 'shelf' configuration at Mach 2.7.

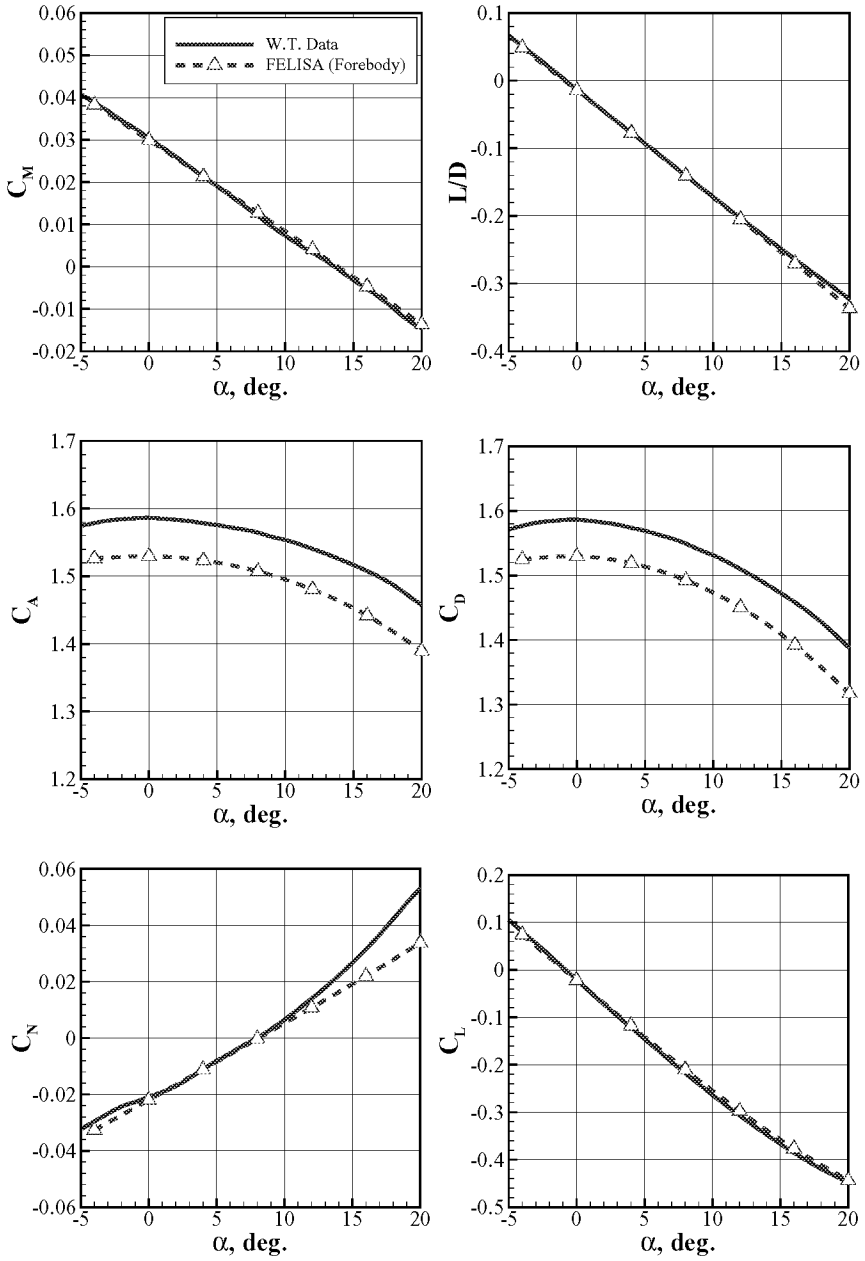

Figure 18: Comparison of aerodynamic data for the 'shelf' configuration at Mach 3.5.

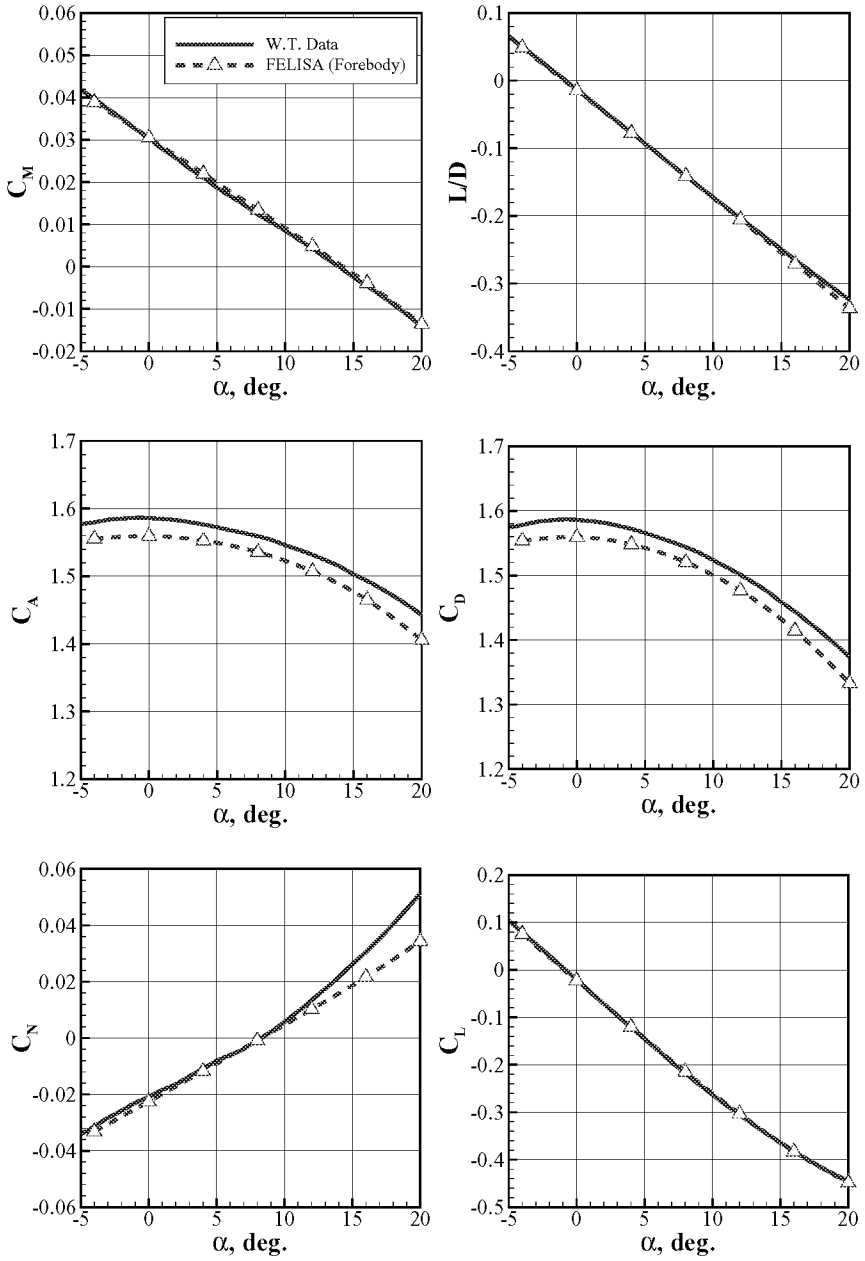

Figure 19: Comparison of aerodynamic data for the 'shelf' configuration at Mach 4.5.

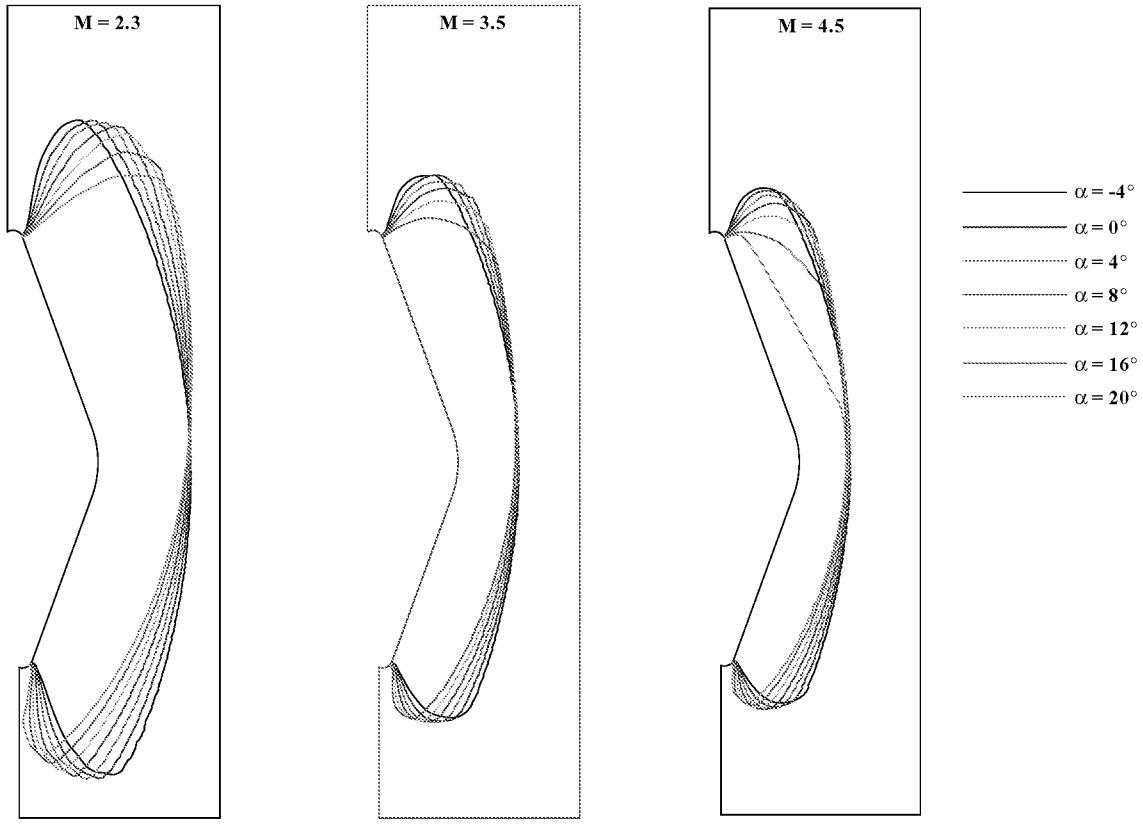

Figure 20: Sonic lines for 'shelf' configuration for Mach 2.3, 3.5, and 4.5.

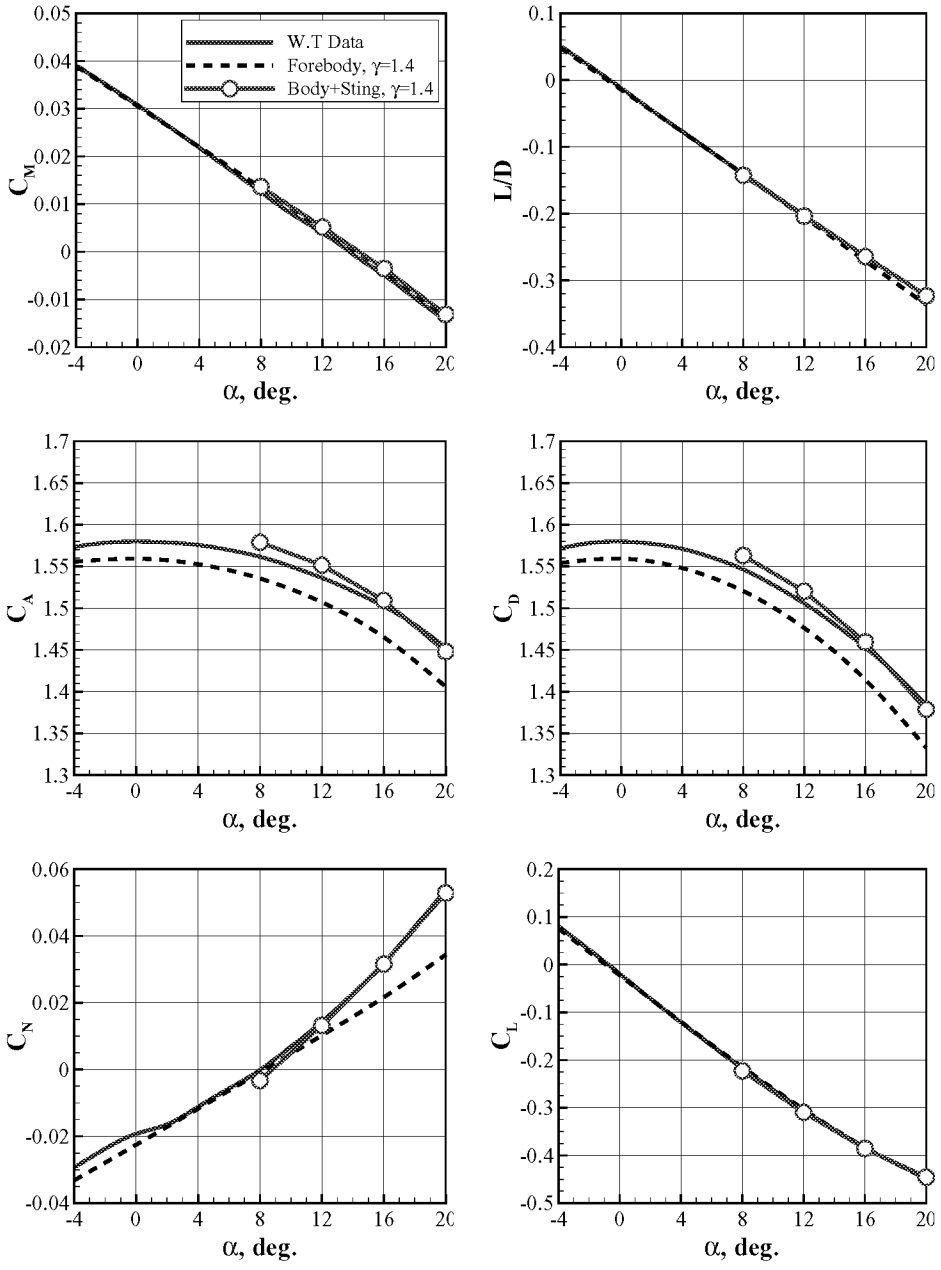

Figure 21: Comparison of aerodynamic data for the 'shelf' configuration at Mach 4.5.

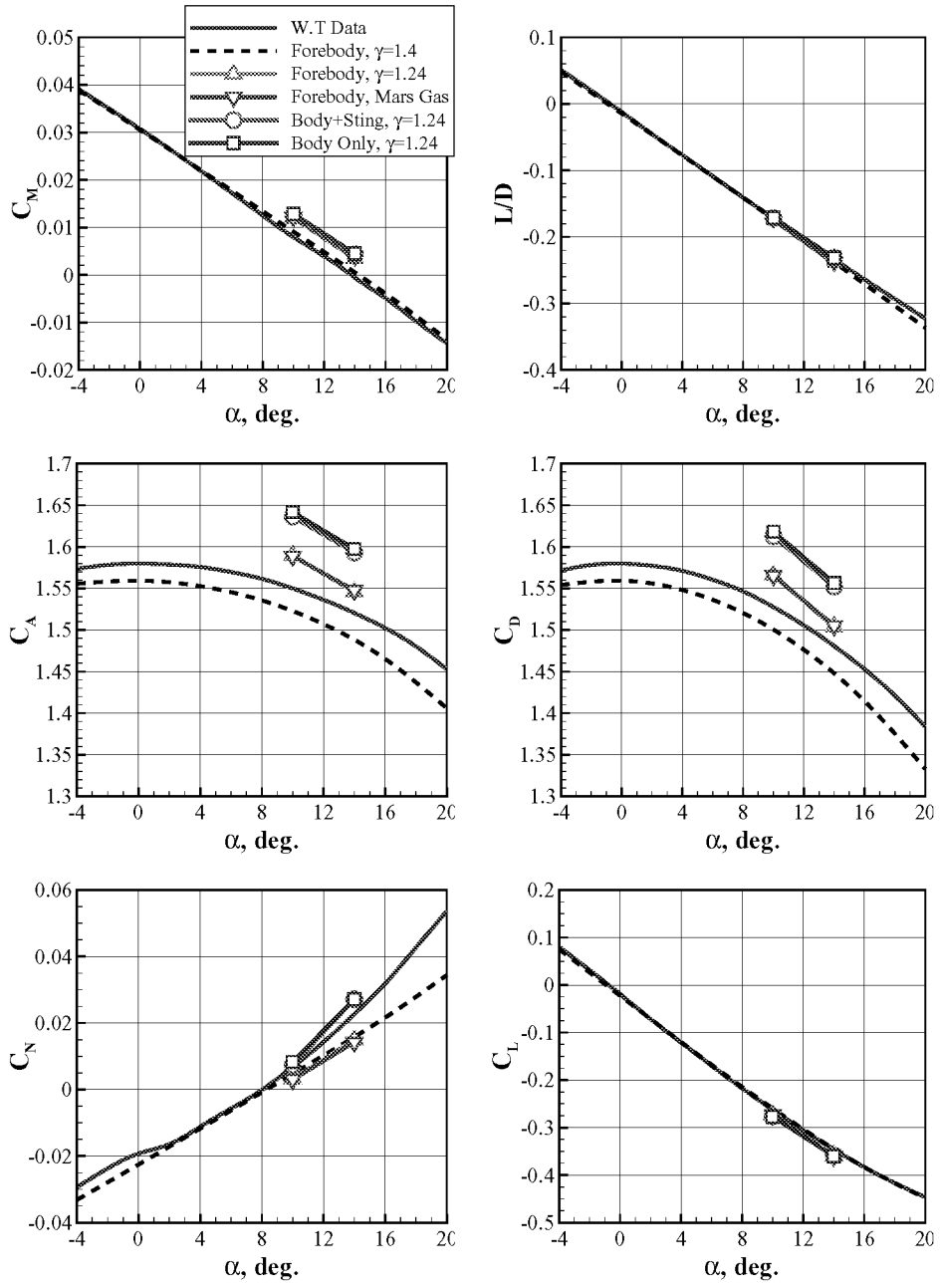

Figure 22: Comparison of aerodynamic data for the 'shelf' configuration at Mach 4.5.

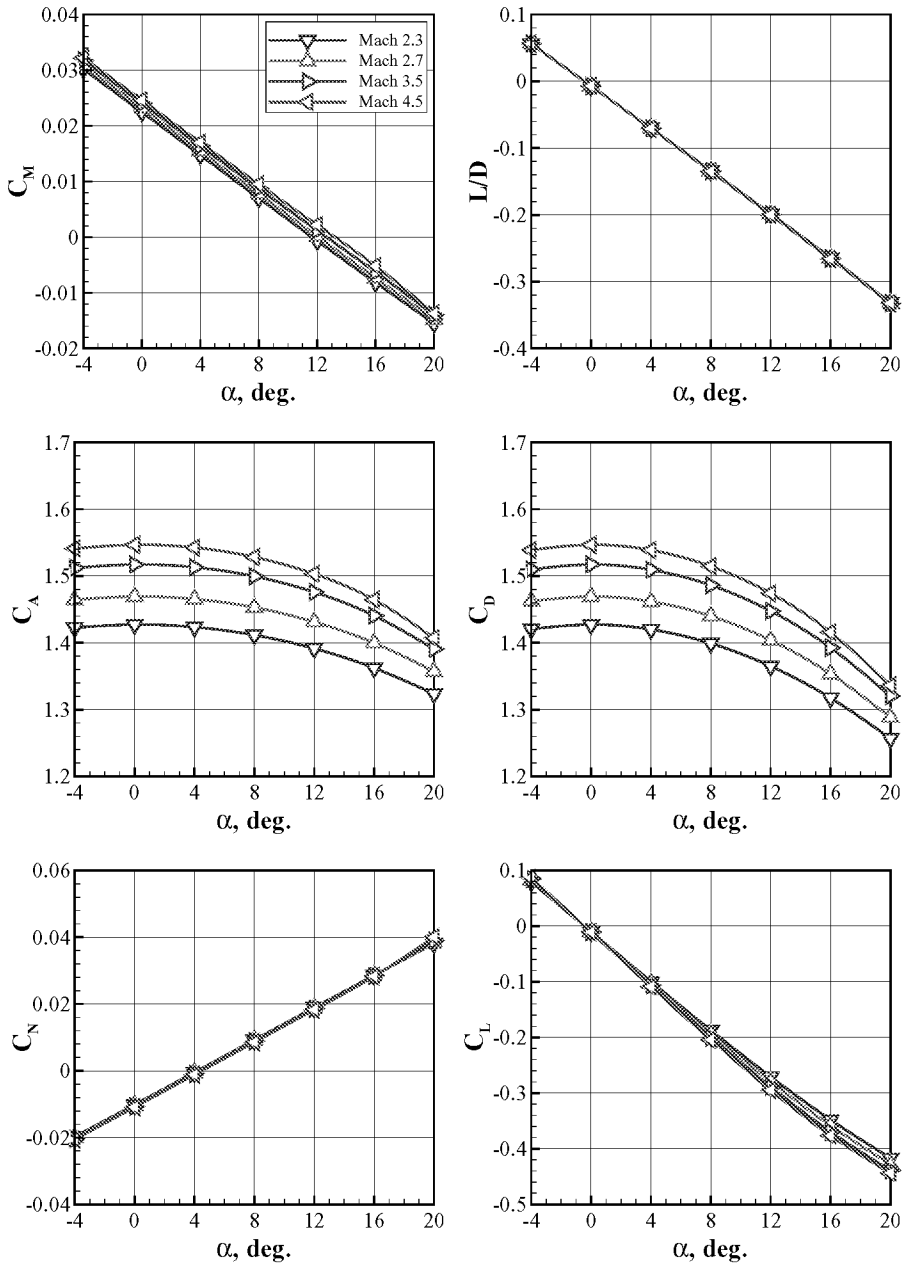

Figure 23: Inviscid aerodynamic data for the 'canted' forebody.

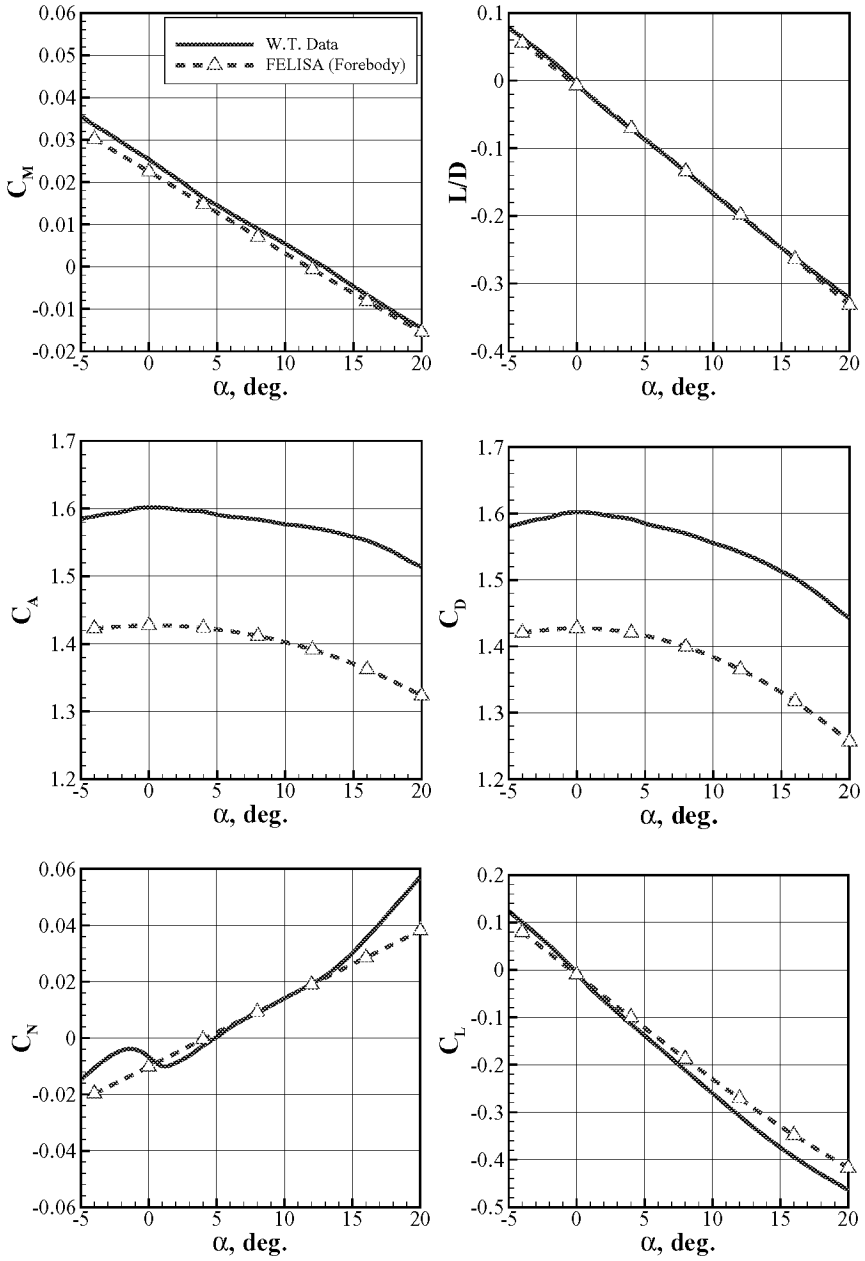

Figure 24: Comparison of aerodynamic data for the 'canted' configuration at Mach 2.3.

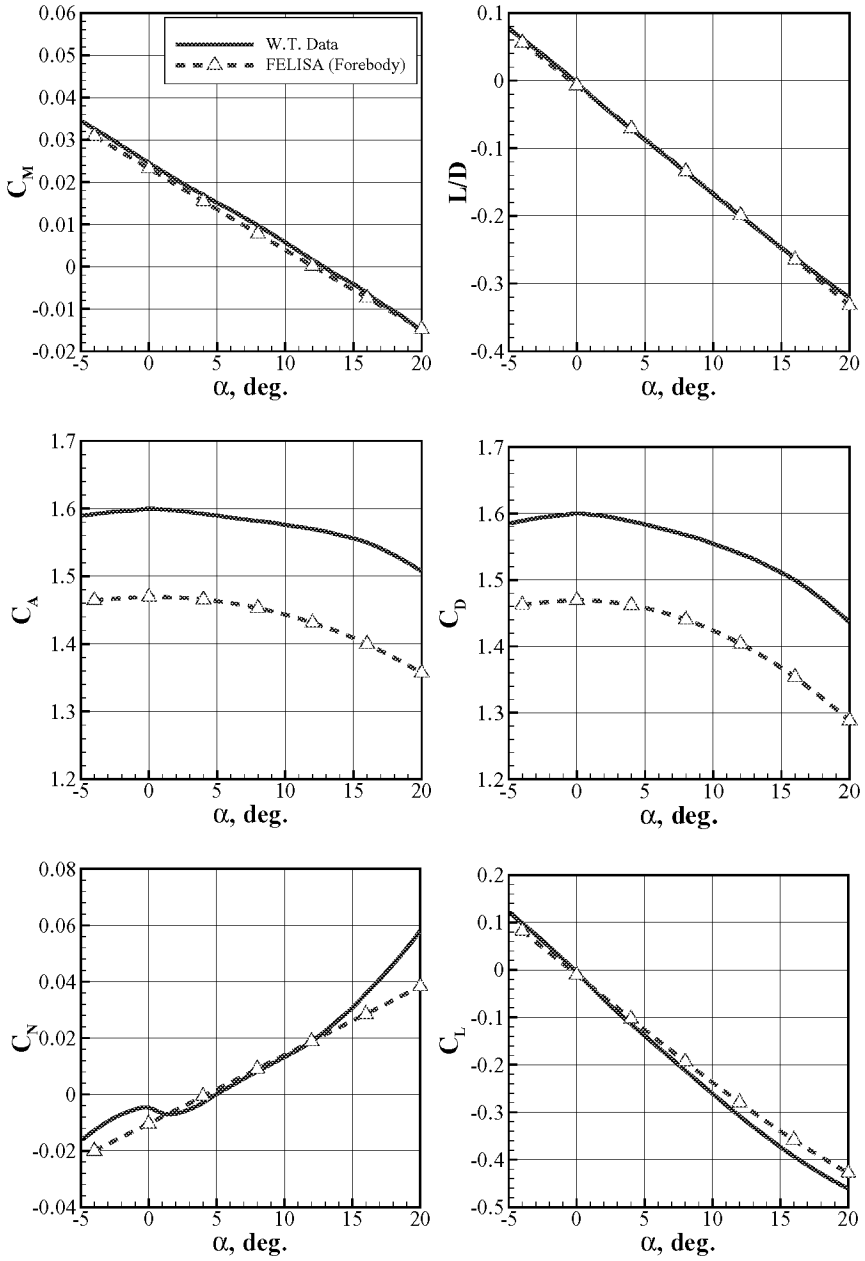

Figure 25: Comparison of aerodynamic data for the 'canted' configuration at Mach 2.7.

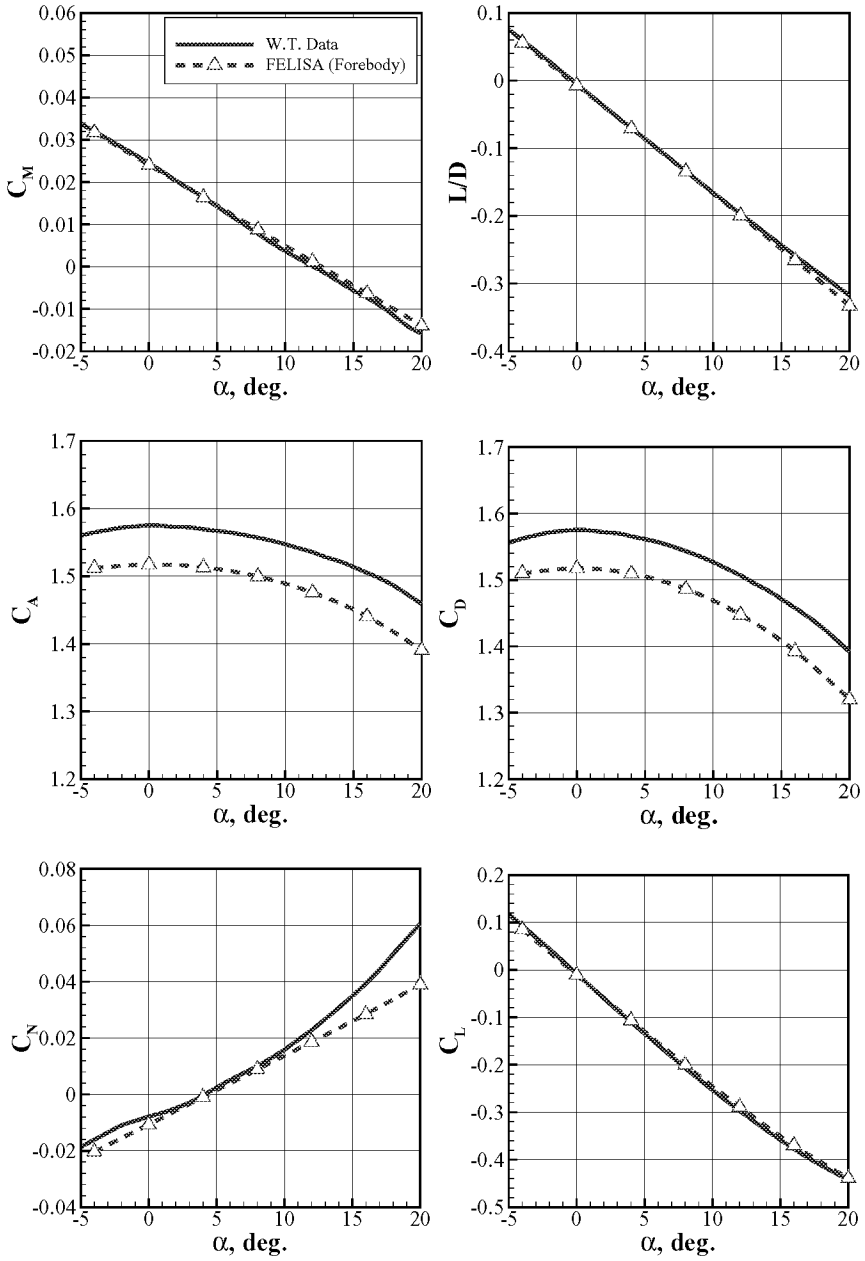

Figure 26: Comparison of aerodynamic data for the 'canted' configuration at Mach 3.5.

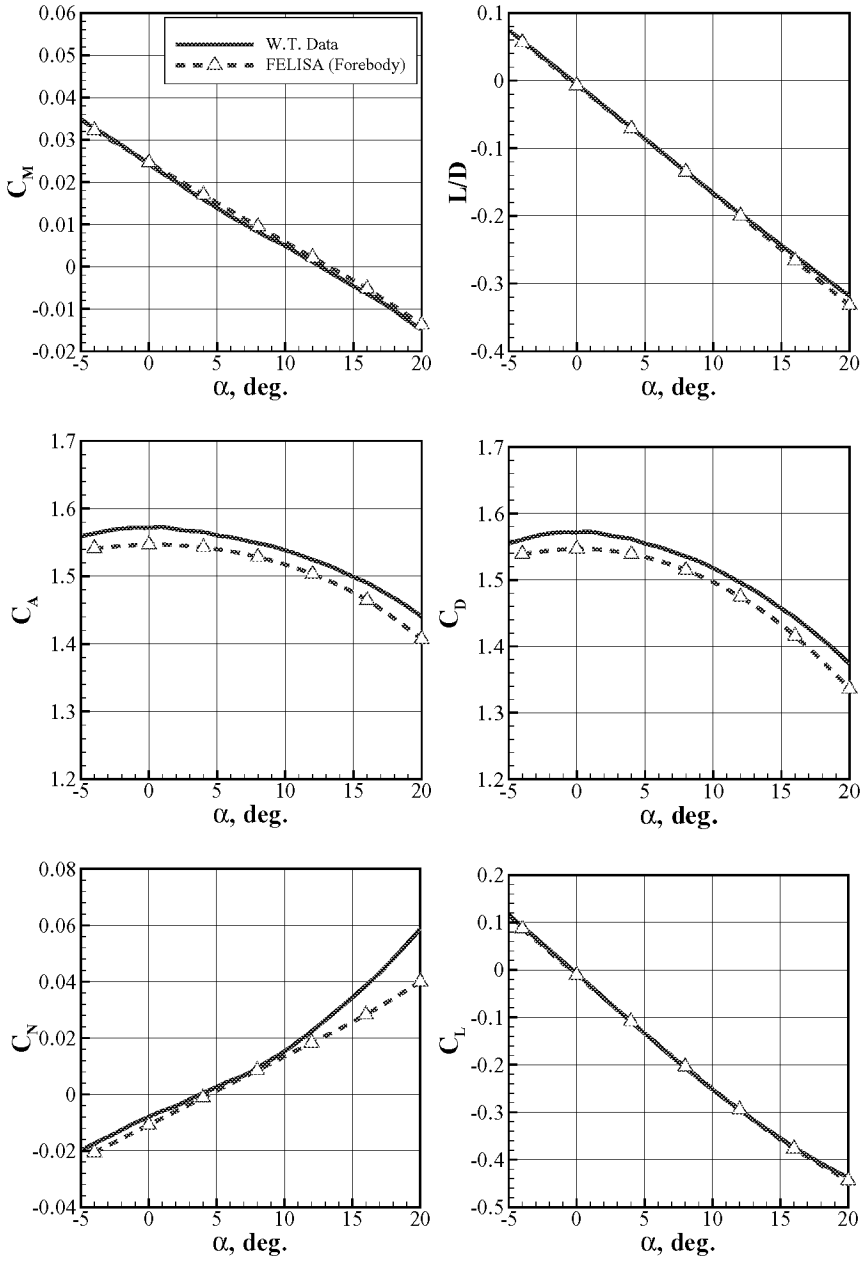

Figure 27: Comparison of aerodynamic data for the 'canted' configuration at Mach 4.5.

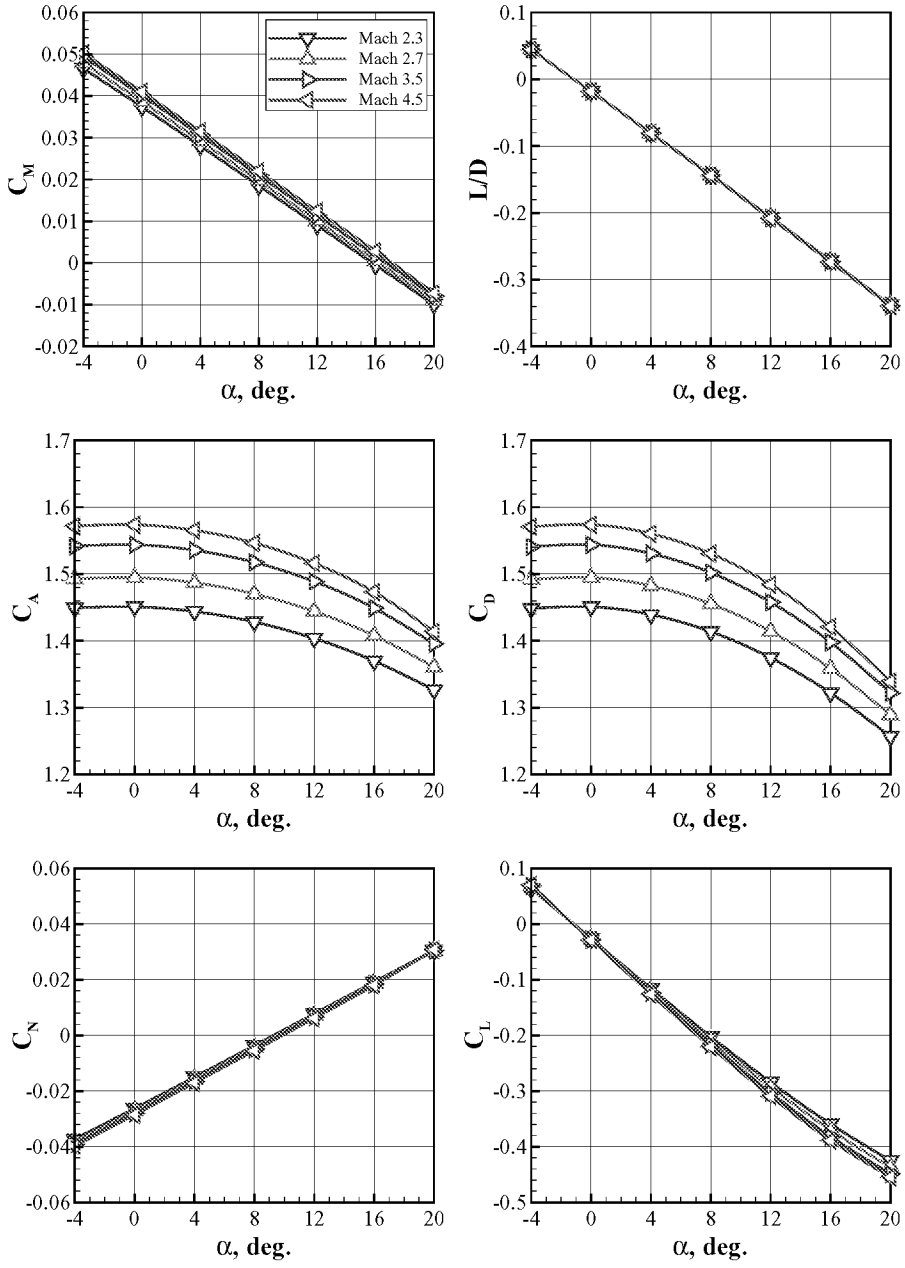

Figure 28: Inviscid aerodynamic data for the 'Ames' forebody.

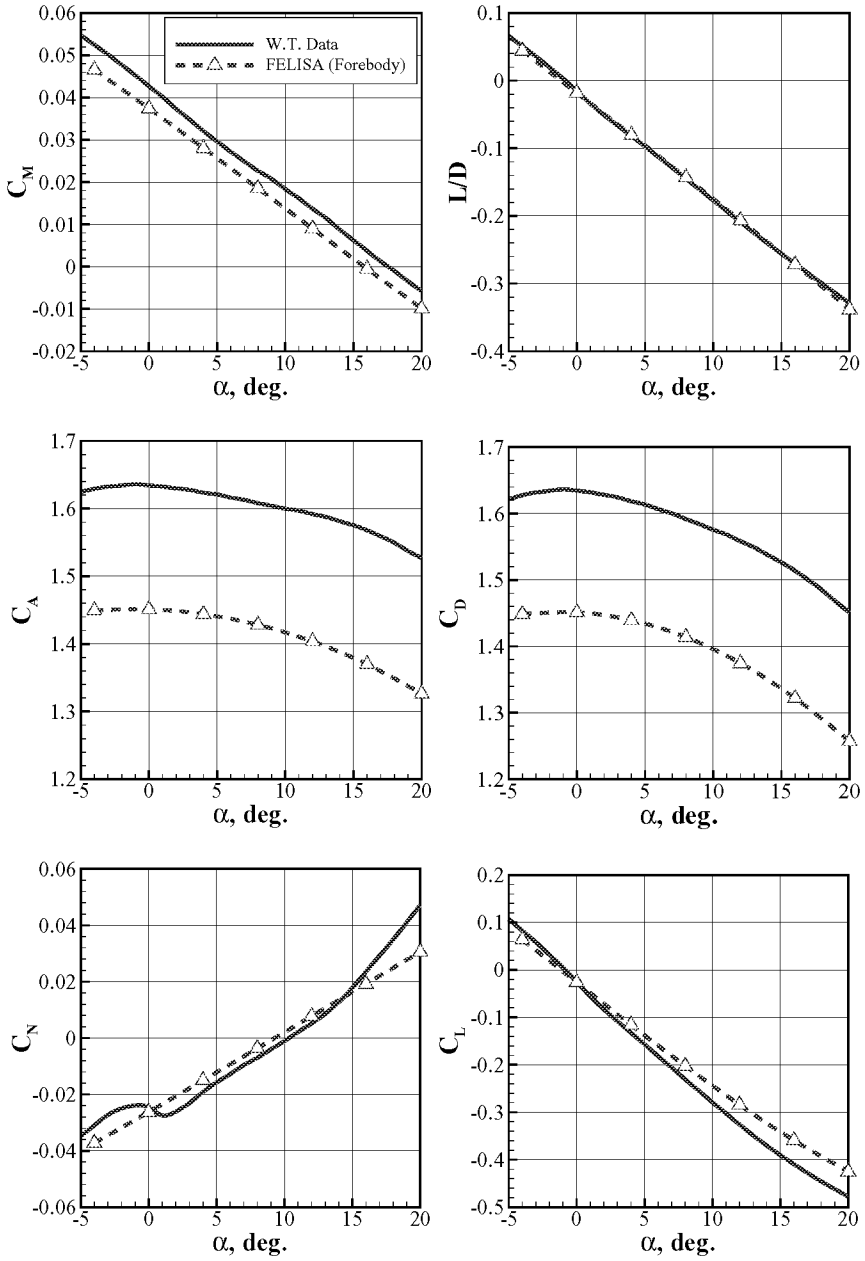

Figure 29: Comparison of aerodynamic data for the 'Ames' configuration at Mach 2.3.

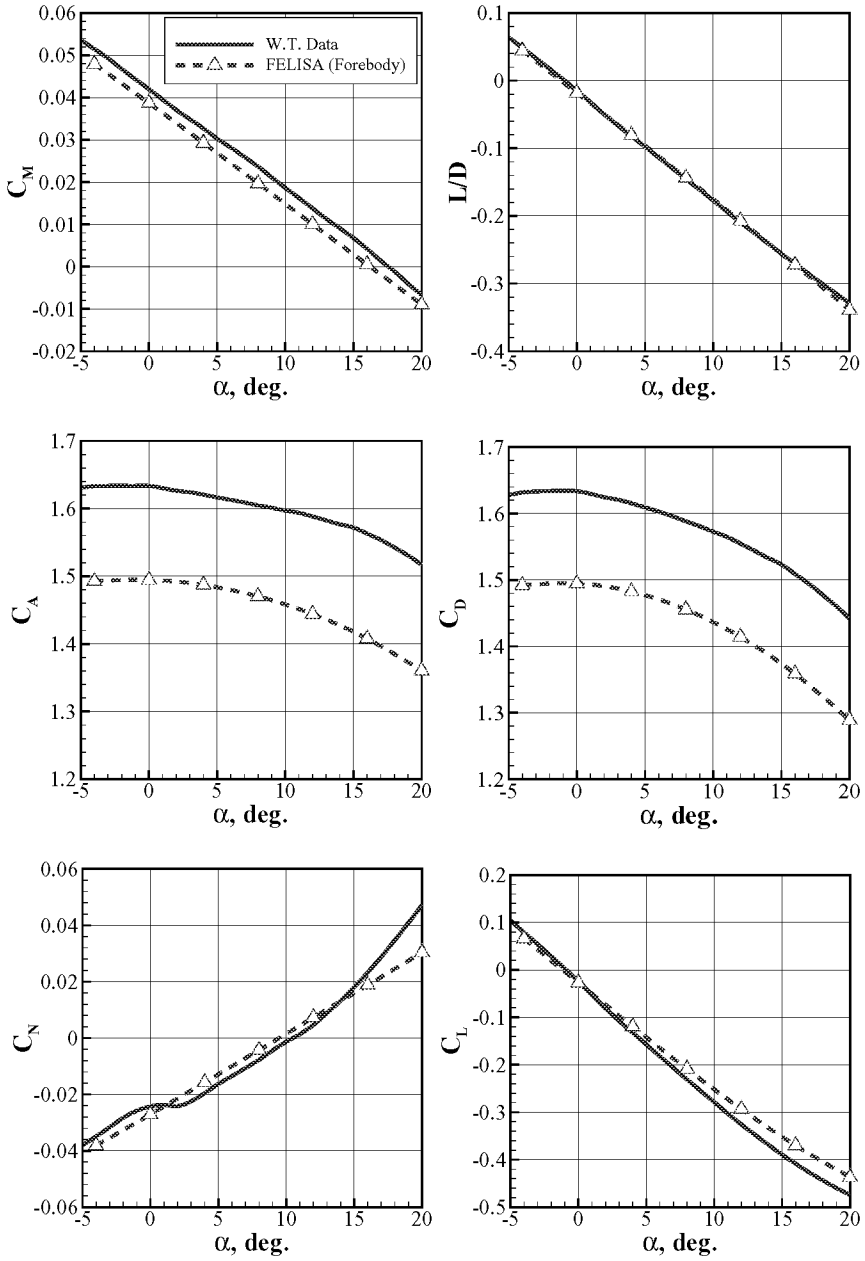

Figure 30: Comparison of aerodynamic data for the 'Ames' configuration at Mach 2.7.

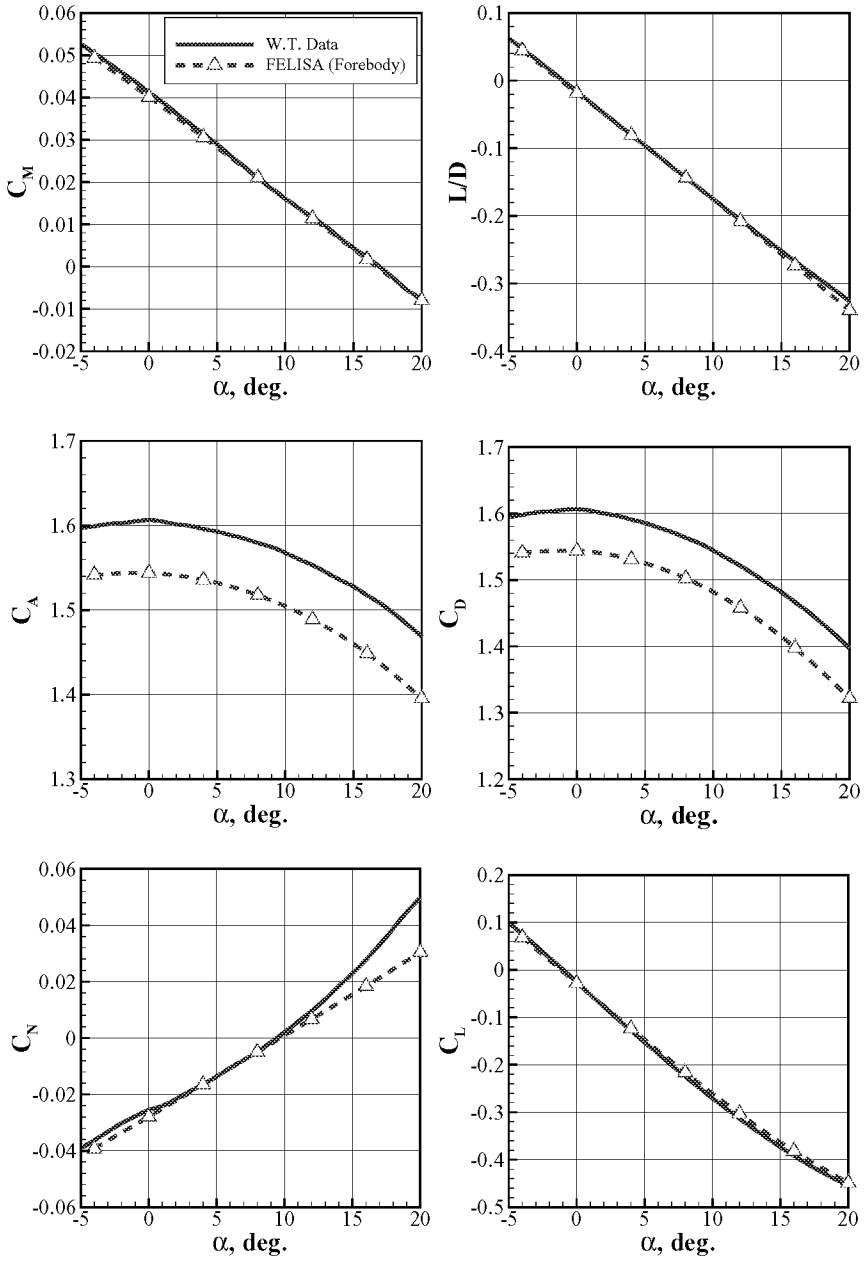

Figure 31: Comparison of aerodynamic data for the 'Ames' configuration at Mach 3.5.

REPORT DOCUMENTATION PAGE

Form Approved
OMB No. 0704–0188

1. AGENCY USE ONLY *(Leave blank)*	2. REPORT DATE	3. REPORT TYPE AND DATES COVERED
	December 2001	Contractor Report

4. TITLE AND SUBTITLE
An Inviscid Computational Study of Three '07 Mars Lander Aeroshell Configurations Over a Mach Number Range of 2.3 to 4.5

5. FUNDING NUMBERS
C NAS1-00135
WU 706-85-41-01

6. AUTHOR(S)
Ramadas K. Prabhu

7. PERFORMING ORGANIZATION NAME(S) AND ADDRESS(ES)
Lockheed Martin Engineering & Sciences Company
C/O NASA Langley Research Center
Hampton, VA 23681–2199

8. PERFORMING ORGANIZATION REPORT NUMBER

9. SPONSORING/MONITORING AGENCY NAME(S) AND ADDRESS(ES)
NASA Langley Research Center
Hampton, VA 23681–2199

10. SPONSORING/MONITORING AGENCY REPORT NUMBER
NASA/CR–2001–211266

11. SUPPLEMENTARY NOTES
Langley Technical Monitor: Kenneth Sutton

12a. DISTRIBUTION/AVAILABILITY STATEMENT
Unclassified-Unlimited
Subject Category 02
Distribution: Nonstandard
Availability: NASA CASI (301) 621–0390

12b. DISTRIBUTION CODE

13. ABSTRACT ***(Maximum 200 words)***

This report documents the results of a study conducted to compute the inviscid longitudinal aerodynamic characteristics of three aeroshell configurations of the proposed '07 Mars lander. This was done in support of the activity to design a smart lander for the proposed '07 Mars mission. In addition to the three configurations with tabs designated as the 'shelf', the 'canted', and the 'Ames', the baseline configuration (without tab) was also studied. The unstructured grid inviscid CFD software FELISA was used, and the longitudinal aerodynamic characteristics of the four configurations were computed for Mach number of 2.3, 2.7, 3.5, and 4.5, and for an angle of attack range of -4 to 20 degrees. Wind tunnel tests had been conducted on scale models of these four configurations in the Unitary Plan Wind Tunnel, NASA Langley Research Center. Present computational results are compared with the data from these tests. Some differences are noticed between the two results, particularly at the lower Mach numbers. These differences are attributed to the pressures acting on the aft body. Most of the present computations were done on the forebody only. Additional computations were done on the full body (forbody and aftbody) for the baseline and the 'Shelf' configurations. Results of some computations done (to simulate flight conditions) with the Mars gas option and with an "effective" γ are also included.

14. SUBJECT TERMS
Unstructured Grid CFD, Hypersonic Speeds, Mars Gas, Aerodynamic Loads

15. NUMBER OF PAGES
47

16. PRICE CODE
A03

17. SECURITY CLASSIFICATION OF REPORT	18. SECURITY CLASSIFICATION OF THIS PAGE	19. SECURITY CLASSIFICATION OF ABSTRACT	20. LIMITATION OF ABSTRACT
Unclassified	Unclassified	Unclassified	UL